

Targeting DCAF5 suppresses *SMARCB1*-mutant cancer by stabilizing SWI/SNF

<https://doi.org/10.1038/s41586-024-07250-1>

Received: 18 October 2022

Accepted: 28 February 2024

Published online: 27 March 2024

 Check for updates

Sandi Radko-Juettner^{1,2,15}, Hong Yue^{3,4,15}, Jacquelyn A. Myers¹, Raymond D. Carter¹, Alexis N. Robertson¹, Priya Mittal¹, Zhexin Zhu¹, Baranda S. Hansen^{5,6}, Katherine A. Donovan^{3,4}, Moritz Hunkeler^{3,4}, Wojciech Rosikiewicz⁷, Zhiping Wu⁸, Meghan G. McReynolds⁸, Shourya S. Roy Burman^{3,4}, Anna M. Schmoker^{3,4}, Nada Mageed³, Scott A. Brown⁹, Robert J. Mobley¹, Janet F. Partridge¹, Elizabeth A. Stewart^{10,11,12}, Shondra M. Pruitt-Miller^{5,6}, Behnam Nabati¹³, Junmin Peng^{8,10}, Nathanael S. Gray¹⁴, Eric S. Fischer^{3,4} & Charles W. M. Roberts^{1,12}

Whereas oncogenes can potentially be inhibited with small molecules, the loss of tumour suppressors is more common and is problematic because the tumour-suppressor proteins are no longer present to be targeted. Notable examples include *SMARCB1*-mutant cancers, which are highly lethal malignancies driven by the inactivation of a subunit of SWI/SNF (also known as BAF) chromatin-remodelling complexes. Here, to generate mechanistic insights into the consequences of *SMARCB1* mutation and to identify vulnerabilities, we contributed 14 *SMARCB1*-mutant cell lines to a near genome-wide CRISPR screen as part of the Cancer Dependency Map Project^{1–3}. We report that the little-studied gene DDB1–CUL4-associated factor 5 (*DCAF5*) is required for the survival of *SMARCB1*-mutant cancers. We show that *DCAF5* has a quality-control function for SWI/SNF complexes and promotes the degradation of incompletely assembled SWI/SNF complexes in the absence of *SMARCB1*. After depletion of *DCAF5*, *SMARCB1*-deficient SWI/SNF complexes reaccumulate, bind to target loci and restore SWI/SNF-mediated gene expression to levels that are sufficient to reverse the cancer state, including *in vivo*. Consequently, cancer results not from the loss of *SMARCB1* function per se, but rather from *DCAF5*-mediated degradation of SWI/SNF complexes. These data indicate that therapeutic targeting of ubiquitin-mediated quality-control factors may effectively reverse the malignant state of some cancers driven by disruption of tumour suppressor complexes.

SWI/SNF chromatin-remodelling complexes hydrolyse ATP to mobilize nucleosomes at enhancers and promoters to regulate DNA accessibility and gene expression⁴. The core subunit *SMARCB1* is essential for the control of enhancer function and cell memory during division⁵, and recent structural studies demonstrate that it acts as an anchor that binds to the nucleosome acidic patch, where it provides leverage for SWI/SNF remodelling activity^{6–9}. Genes encoding SWI/SNF subunits are mutated in nearly 25% of cancers^{4,10}. Inactivation of the SWI/SNF subunit *SMARCB1* occurs in several aggressive cancer types, including rhabdoid tumours (RTs) and sarcomas^{10–12}. *SMARCB1* is a bona fide tumour suppressor, as germline mutations predispose to cancer, and its deletion in mice results in rapid onset cancer in all mice^{4,13}. RTs have simple diploid genomes, with the loss of *SMARCB1* typically being the sole identified driver mutation^{7,10}. As the *SMARCB1* tumour suppressor

protein is absent, the sole driving mutation cannot be directly therapeutically targeted. As a consequence, identifying genetic vulnerabilities specific to *SMARCB1*-mutant cells has the potential to both yield insights into the mechanisms through which *SMARCB1* loss promotes cancer and to inform therapeutic approaches.

The Cancer Dependency Map Project (DepMap) is a large-scale collaboration that leverages hundreds of cancer cell lines to systematically identify genetic dependencies, small-molecule sensitivities and identify the biomarkers that predict them. To search for genetic vulnerabilities in *SMARCB1*-mutant cancers, we contributed 14 *SMARCB1*-mutant RT lines to DepMap for near genome-wide CRISPR–Cas9 loss-of-function screening^{1–3}. Using the data from the screen, we identified *DCAF5*, a substrate receptor for the CUL4–DDB1 E3 ubiquitin protein ligase complex^{14–16}, as a specific dependency in *SMARCB1*-deficient RT cell

¹Division of Molecular Oncology, Department of Oncology, St Jude Children's Research Hospital, Memphis, TN, USA. ²St Jude Graduate School of Biomedical Sciences, St Jude Children's Research Hospital, Memphis, TN, USA. ³Department of Cancer Biology, Dana-Farber Cancer Institute, Boston, MA, USA. ⁴Department of Biological Chemistry and Molecular Pharmacology, Harvard Medical School, Boston, MA, USA. ⁵Department of Cell and Molecular Biology, St Jude Children's Research Hospital, Memphis, TN, USA. ⁶The Center for Advanced Genome Engineering, St Jude Children's Research Hospital, Memphis, TN, USA. ⁷Center for Applied Bioinformatics, St Jude Children's Research Hospital, Memphis, TN, USA. ⁸Department of Structural Biology, St Jude Children's Research Hospital, Memphis, TN, USA. ⁹Department of Immunology, St Jude Children's Research Hospital, Memphis, TN, USA. ¹⁰Department of Developmental Neurobiology, St Jude Children's Research Hospital, Memphis, TN, USA. ¹¹Department of Oncology, St Jude Children's Research Hospital, Memphis, TN, USA. ¹²Cancer Center, St Jude Children's Research Hospital, Memphis, TN, USA. ¹³Human Biology Division, Fred Hutchinson Cancer Center, Seattle, WA, USA. ¹⁴Department of Chemical and Systems Biology, ChEM-H, Stanford Cancer Institute, Stanford Medicine, Stanford, CA, USA. ¹⁵These authors contributed equally: Sandi Radko-Juettner, Hong Yue. [✉]e-mail: eric_fischer@dfci.harvard.edu; charles.roberts@stjude.org

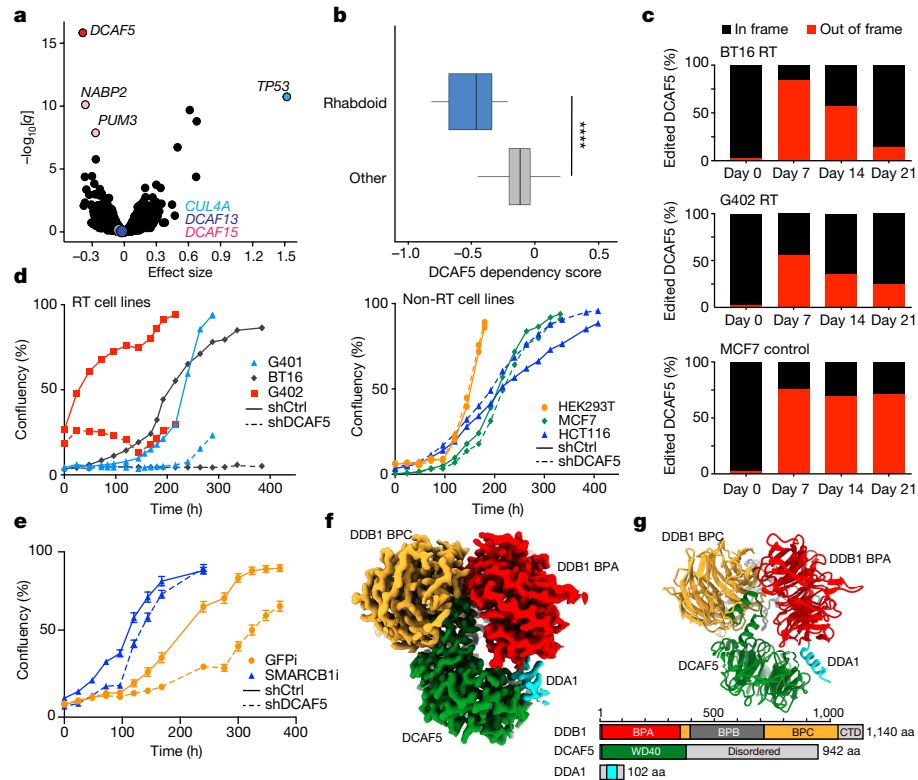


Fig. 1 | DCAF5 is a specific dependency in SMARCB1-mutant cancers.

a. Comparison of $n = 14$ biologically independent RT cell lines to $n = 789$ biologically independent other cancer cell lines from DepMap (release CERES 21Q1). Each circle represents a single gene. A negative effect size indicates that RT cells are preferentially dependent on that gene. $-\log_{10}[q]$ was calculated from empirical-Bayes-modulated t -statistics with Benjamini–Hochberg correction. **b.** Two-class comparison of $n = 14$ biologically independent RT cell lines to $n = 789$ biologically independent other cancer cell lines. Statistical analysis was performed using a two-tailed Student's t -test; $****P = 8.21 \times 10^{-21}$. Release CERES 21Q1. The box plot shows the median (centre line), the third and first quartiles (box limits) and $1.5 \times$ interquartile range above and below the box (whiskers). **c.** Indel toxicity assay. DCAF5 was targeted with a CRISPR guide to generate mutations. Then, selective pressure against out-of-frame mutations (containing DCAF5 knockout) was measured over time in BT16 and G402 RT cells and control MCF7 cells. **d.** The effects of DCAF5 shRNA knockdown on the

proliferation of SMARCB1-mutant cell lines or SMARCB1-expressing control cell lines. The solid lines show shCtrl and the dotted lines show shDCAF5. Data are mean values from $n = 8$ technical replicates per cell line condition from one independent experiment. **e.** The proliferation of SMARCB1-knockout HEK293T cells after knockdown of DCAF5 and re-expression of SMARCB1 or GFP (control). The solid lines show shCtrl and the dotted lines show shDCAF5. Data are mean values from $n = 16$ technical replicates per cell line condition from one independent experiment. **f.** Cryo-EM map (post-processed using deepEMhancer) of the DCAF5–DDB1(ΔB)–DDA1 complex segmented to indicate DDA1 (cyan), DCAF5 (green), DDB1 BPC (orange), DDB1 BPA (red) and DDB1 C-terminal domain (grey). **g.** Cartoon representation of the DCAF5–DDB1(ΔB)–DDA1 complex. Domain representation of the proteins present in the complex. Regions omitted from the constructs (BPB) are indicated in dark grey. aa, amino acids; CTD, C-terminal domain.

lines ($P < 10^{-21}$; Fig. 1a,b). Dependency on DCAF5 for survival was not seen in other SWI/SNF mutant cancers (Extended Data Fig. 1a). DCAF5 is one of around 20 members of the DDB1–CUL4-associated factor (DCAF) family^{17,18} that function as substrate receptors for cullin–RING E3-ubiquitin ligase complexes, which target specific proteins for ubiquitylation and degradation^{16,19}. DCAF5 is widely expressed and dependency did not correlate with DCAF5 expression levels (Extended Data Fig. 1b,c). We validated DCAF5 dependency by performing CRISPR-based competitive fitness assays (Fig. 1c) and short hairpin RNA (shRNA)-mediated knockdown (Fig. 1d and Extended Data Fig. 1d). In both cases, the loss of DCAF5 caused strong selection against SMARCB1-deficient RT cells but not control cell lines. RT cells in which DCAF5 had been knocked down often began regrowing after several days concomitant with loss of DCAF5 silencing over time (Extended Data Fig. 1e). Furthermore, we were unable to generate DCAF5-deficient clones of RT cell lines using CRISPR to knock out DCAF5, but were able to do so with control MCF7 lines. To confirm that the DCAF5 dependency was directly caused by the absence of SMARCB1, we developed an isogenic HEK293T cell model in which we knocked out SMARCB1 using CRISPR–Cas9 and then engineered these cells to re-express SMARCB1 inducibly²⁰. Knockdown of DCAF5 had no effect on SMARCB1-expressing HEK293T cells

but impaired the proliferation of SMARCB1-deficient HEK293T cells (Fig. 1e). Collectively, these data demonstrate that DCAF5 becomes essential for cell survival in the absence of SMARCB1.

DCAF5 is known to interact with components of the CUL4–DDB1 (CRL4) E3-ubiquitin ligase complex, which promotes proteasome-directed protein degradation^{14–16,19}. This is also the case in RT cells as immunoprecipitated DCAF5 co-precipitated DDB1 and CUL4A (Extended Data Fig. 1f), suggesting that the degradation of an unknown DCAF5 target(s) may be required for the viability of SMARCB1-deficient cells. To further establish DCAF5 as a bona fide substrate receptor of a CRL4–DCAF5 ligase complex, we determined the cryogenic electron microscopy (cryo-EM) structure of the DCAF5–DDB1(ΔB1)–DDA1 complex at a resolution of 2.6 Å (Fig. 1f,g and Extended Data Figs. 2 and 3 and Extended Data Table 1). DCAF5 tightly interacts with DDB1 through a canonical helix-loop-helix motif (Extended Data Fig. 3a, b). Furthermore, DDA1, a common component associated with CRL4 complexes²¹, intercalates a β-strand in the DDB1 propeller (BPA) through several conserved residues, and the C terminus of DDA1 forms an α-helix that binds to DCAF5 through hydrophobic interactions, further stabilizing the complex (Extended Data Fig. 3c). Our high-resolution cryo-EM structure reveals the presence

Article

of a canonical and evolutionarily conserved WD40 β -propeller repeat domain within DCAF5 (Fig. 1f,g and Extended Data Fig. 3d) that is predicted to function as the substrate-binding site²².

Loss of SMARCB1 is known to disrupt the integrity of the SWI/SNF complex, leading to reduced protein levels of several SWI/SNF subunits, an effect that is post-translational as it was rescued by treatment with the proteasome inhibitor MG132²³. We therefore hypothesized that, in the absence of SMARCB1, DCAF5 promotes the degradation of malformed SWI/SNF complexes and that accumulation of defective complexes in the absence of DCAF5 may be toxic due to interference with transcription.

To test whether DCAF5 regulates SWI/SNF subunit levels, we performed western blot analysis of G401 and TTC549 RT cells treated with either control shRNA (shCtrl) or shRNA against *DCAF5* (shDCAF5). Knockdown of *DCAF5* resulted in increased levels of the SWI/SNF subunits ARID1A, SMARCA4, PBRM1 and SMARCC1, but had little effect in control *SMARCB1*-wild-type HCT116 cells (Fig. 2a,b and Extended Data Fig. 4a). *DCAF5* knockdown in SMARCB1-deficient HEK293T cells increased the levels of the same SWI/SNF subunits, an effect that was eliminated by expression of SMARCB1 (Fig. 2c). There were no changes in transcript levels for SWI/SNF subunits, and increased levels of SWI/SNF subunits after *DCAF5* loss also occurred in the presence of cycloheximide, indicating that increases occurred post-translationally (Extended Data Fig. 4b,c). Furthermore, the decay rates for SWI/SNF subunits were significantly slower in the absence of DCAF5, indicating that DCAF5 regulates the stability of SWI/SNF substrates (Extended Data Fig. 4c).

SMARCB1 is present in two out of the three different SWI/SNF complexes (cBAF and PBAF) but is absent from the third (ncBAF (also known as GBAF)), which is defined by the presence of BRD9^{20,24,25}. In contrast to the cBAF and PBAF complexes, in which the ARID1A, SMARCA4, PBRM1 and SMARCC1 subunits increased after *DCAF5* knockdown, the levels of BRD9 (in ncBAF) were unaffected by *DCAF5* loss (Fig. 2a and Extended Data Fig. 4a). To directly evaluate whether the absence of SMARCB1 caused DCAF5-mediated degradation of SWI/SNF subunits, we re-expressed SMARCB1 in RT cell lines G401, TTC549 and in SMARCB1-deficient HEK293T cells. We observed that the effect of *DCAF5* loss was substantially reduced in all models in the presence of SMARCB1 (Fig. 2a,c and Extended Data Fig. 4a).

To evaluate the effect of *DCAF5* knockdown on SWI/SNF complex assembly, we performed glycerol gradient fractionation of lysates from RT cell lines in which expression of *SMARCB1* is inducible (G401^{SMARCB1i} and BT16^{SMARCB1i}). After *DCAF5* knockdown, the levels of ARID1A, SMARCA4 and PBRM1 increased in both smaller fractions, representing partially assembled complexes, and in full-size (other than SMARCB1) complexes (Fig. 2d and Extended Data Fig. 4d). Induction of SMARCB1 in both G401^{SMARCB1i} and BT16^{SMARCB1i} cells resulted in a shift of SWI/SNF subunits into fractions of higher density and again abrogated the effect of *DCAF5* loss. To further evaluate whether the increased SMARCA4 protein is assembled into SWI/SNF complexes, we performed SMARCA4 immunoprecipitation (IP)-western blot and IP-mass spectrometry (IP-MS) experiments. Despite protein levels of SMARCA4 increasing after *DCAF5* loss, the ratio of SMARCA4 associated with cBAF and PBAF subunits was maintained after *DCAF5* loss (Extended Data Fig. 4e,f and Supplementary Table 1). Collectively, these data demonstrate that, in RT cells, DCAF5 inactivation results in increased the levels of partially and fully assembled cBAF and PBAF complexes that lack SMARCB1.

To determine whether degradation of SWI/SNF subunits was a direct or indirect function of DCAF5, we immunoprecipitated DCAF5 in RT cells. Together with known interactors CUL4A and DDB1, the SWI/SNF subunits ARID1A, SMARCA4, PBRM1 and SMARCC1 immunoprecipitated with DCAF5, whereas subunits of ncBAF (BRD9 and GLTSCR1) did not (Fig. 2e). Reverse IP confirmed these results, as SMARCA4 co-purified DCAF5 (Extended Data Fig. 4g). Thus, the absence of SMARCB1 causes DCAF5 to bind to and reduce the levels of specific

SWI/SNF subunits belonging to complexes that normally contain SMARCB1. Exogenous expression of cBAF and DCAF5-DDB1 in Expi293 cells followed by affinity purification further corroborated the interaction between DCAF5 and the cBAF complex (Fig. 2f).

It has recently been reported that the adapter protein L3MBTL3 and the demethylase LSD1 (encoded by *KDM1A*) have a role in targeting SWI/SNF subunits for ubiquitylation²⁶ and we therefore evaluated whether either L3MBTL3 or LSD1 are specific dependencies in RT cell lines. Analysis of DepMap data revealed that *L3MBTL3* was not a dependency in RT cell lines (Extended Data Fig. 4h). *KDM1A* knockout caused a mild reduction in the proliferation of nearly all cell lines in DepMap, an effect that trended toward being slightly less pronounced in RT cells. Consequently, in contrast to *DCAF5*, neither of these genes are specific RT cell dependencies. We next evaluated biochemical interactions between L3MBTL3 and DCAF5. Immunoprecipitates of L3MBTL3 did not co-precipitate DCAF5 or SWI/SNF proteins in G401 RT cells (Extended Data Fig. 4i). Moreover, in the DCAF5 quantitative IP-MS experiments conducted in G401 and HEK293T cells, we did not observe any interaction with L3MBTL3 (Supplementary Tables 2 and 3). Subsequently, we evaluated whether knockdown of *L3MBTL3* or *KDM1A* alters the levels of SWI/SNF proteins in a manner similar to the loss of *DCAF5*. We observed no difference in the abundance of SWI/SNF proteins levels after depletion of *L3MBTL3* or *KDM1A* in RT cells (Extended Data Fig. 4j,k). We next focused our efforts on the methylated lysine residues Lys201, 482 and 615 (SMARCC1) and Lys328, 457 and 592 (SMARCC2), which were reported to be recognized for degradation by L3MBTL3²⁶. We used biochemistry, proteomics and open-access data resources to investigate these residues and found no evidence of methylation. In G401 and HEK293T cells, MS analysis revealed no evidence of lysine methylation at residues Lys201/482/615/328/457/592 in SMARCC1/SMARCC2 and further analysis from PhosphositePlus and MethylSight confirmed the absence of these methylation events (Supplementary Tables 4 and 5). Collectively, our extensive analyses demonstrate that L3MBTL3 and LSD1 are dispensable for the regulation of SWI/SNF subunits by CRL4-DCAF5 in RT cells.

To determine whether DCAF5 was specific for SWI/SNF subunits or whether it has broader effects on proteome activity in the absence of SMARCB1, we used the degradation TAG (dTAG) system^{27,28}. An FKBP12(F36V)-2 \times HA-tagged DCAF5 was degraded with as little as 50 nM of the dTAG^{V-1} inducer (Fig. 3a and Supplementary Fig. 2a-d). Degradation occurred within 30 min and was sustained for at least 72 h (Fig. 3b). Cells treated with either DMSO or dTAG^{V-1} for 24 h were analysed using tandem mass tag (TMT) quantification. Comparing dTAG^{V-1}-treated cells with DMSO control revealed that the effect of DCAF5 loss was largely specific for SWI/SNF complex members: of the top 18 proteins that increased in abundance, 9 were components of the cBAF and PBAF SWI/SNF complexes (Fig. 3c and Supplementary Table 6), whereas ncBAF complex members were unaffected.

To evaluate whether DCAF5 is directly involved in the ubiquitylation of SWI/SNF subunits, we performed in vitro ubiquitylation assays. We screened a library of 13 E2 enzymes and identified 4 that facilitate DCAF5 autoubiquitylation (Extended Data Fig. 5a): UBE2D1, UBE2D2, UBE2D3 and UBE2D4. To evaluate the activity of DCAF5, we used SMARCC1 as a model substrate, given that its abundance was most upregulated after DCAF5 degradation (Fig. 3c) and given its importance to the structural integrity of the SWI/SNF complex²⁹. DCAF5 was capable of directly polyubiquitylating SMARCC1 in vitro (Extended Data Fig. 5b). Through sequence alignments, we observed that the bottom face of the WD40 domain is markedly conserved (Extended Data Fig. 3e), suggesting a role in substrate recognition. We next used three CRL4-DCAF5 constructs: DCAF5(1-477) (containing only the helix-loop-helix (HLH) motif and the WD40 domain), DCAF5(1-601) (containing an extended region) and full-length DCAF5, alongside the CRL4-DCAF11 complex (another RINGE3 ligase) as a negative control and the whole recombinant SWI/SNF complex for ubiquitylation (Extended Data Fig. 5c-f). Western

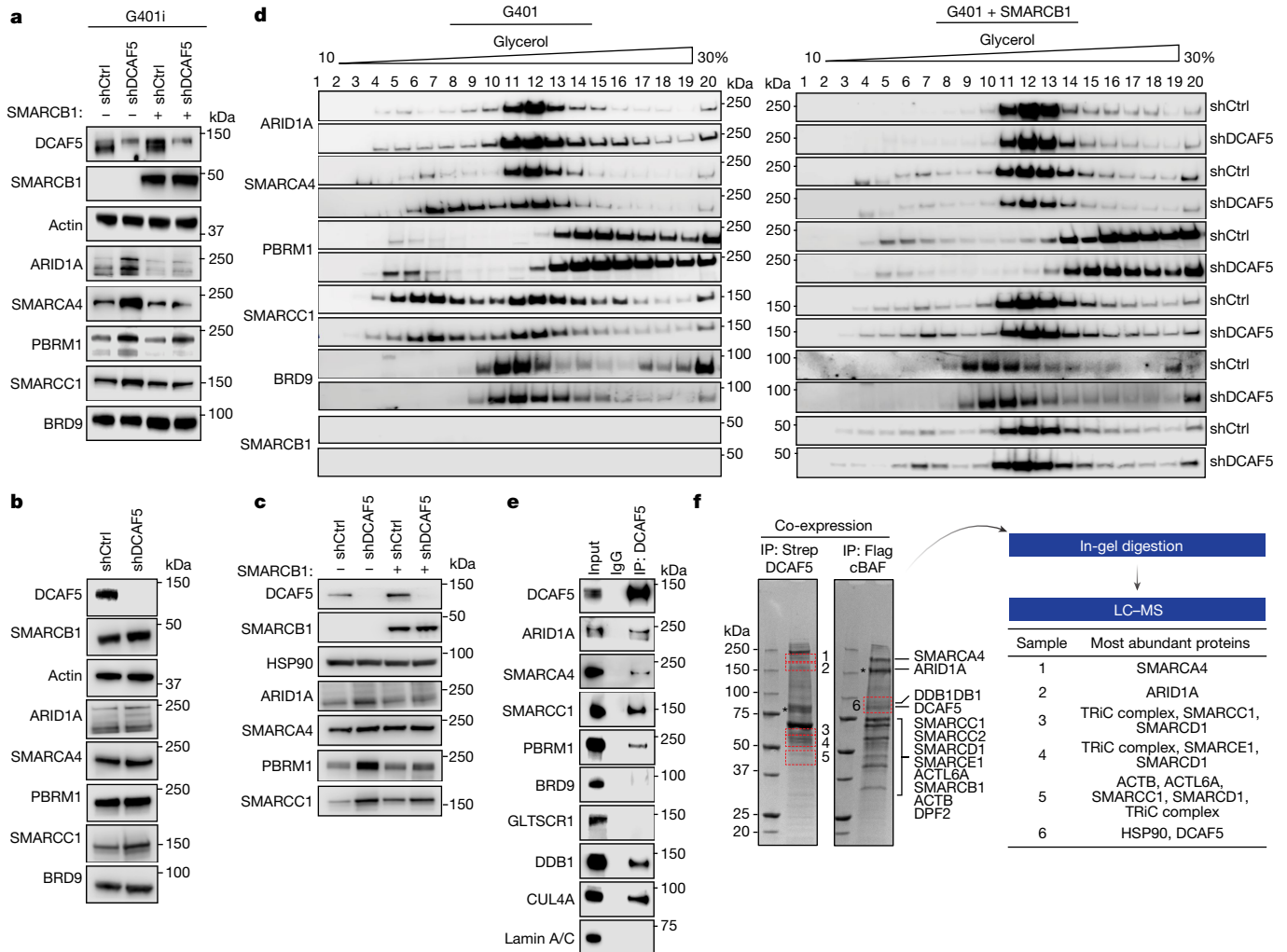


Fig. 2 | DCAF5 targets SWI/SNF subunits for degradation in SMARCB1-deficient cells. **a**, Western blot analysis of SWI/SNF subunits in G401 SMARCB1-deficient RT cells treated with shCtrl or shDCAF5 (lanes 1 and 2) or in RT cells in which SMARCB1 was re-expressed (lanes 3 and 4) after 72 h selection. **b**, Western blot analysis of SWI/SNF subunits in control (*SMARCB1* wild type) HCT116 cells treated with shCtrl or shDCAF5 after 72 h selection. **c**, Western blot analysis of SWI/SNF subunits in *SMARCB1*-knockout HEK293T cells after knockdown of *DCAF5* and re-expression of *SMARCB1* or GFP (control). **d**, Glycerol gradient (10–30% glycerol) of SMARCB1-deficient G401 RT cells treated with either shCtrl or shDCAF5 after 72 h selection (left). Right, SMARCB1

re-expressed cells. **e**, DCAF5 co-immunoprecipitation in G401 RT cells, blotting for DCAF5 and known E3 ubiquitin ligase interactors (positive controls) and SWI/SNF subunits. Lamin A/C was used as a negative control. The input is 1% of the protein used for the IP. **f**, Reciprocal pull-down assays of DCAF5 and the cBAF complex. The experiment was performed once. The asterisks indicate bait proteins. DCAF5 was tagged with a Strep-tag II and purified using Strep-TactinXT beads (left). cBAF was Flag-tagged on ARID1A and purified using anti-Flag antibodies (right). Data are representative of three (**a** and **b**) or two (**c**–**e**) independent biological experiments. LC-MS, liquid chromatography-mass spectrometry.

blot analysis revealed that both SMARCC1 and SMARCA4 are ubiquitylated by DCAF5 (Extended Data Fig. 5c,d), with the strongest activity from the DCAF5(1–477) construct, confirming that the WD40 domain has a function in substrate recognition (Extended Data Fig. 5c,d). AlphaFold2-Multimer³⁰ co-folding predictions of DCAF5 with individual SWI/SNF subunits also suggest that DCAF5 primarily interacts with SWI/SNF through its WD40 domain (Extended Data Fig. 3f).

To complement our *in vitro* studies, we performed di-Gly proteomics³¹ in SMARCB1-deficient G401 RT cells with and without DCAF5 to identify which SWI/SNF substrates are ubiquitylated in living cells. We identified a total of 21,555 di-Gly sites on 4,951 proteins. Ubiquitylation of multiple lysines on SMARCA4, ARID1A and SMARCC1 were all dependent on DCAF5 (Fig. 3d and Extended Data Fig. 5g–i and Supplementary Tables 7 and 8). Collectively, these data demonstrate that DCAF5 directly promotes ubiquitylation and degradation of SWI/SNF subunits.

We postulated that if, in the absence of both DCAF5 and SMARCB1, the elevated levels of uncomplexed SWI/SNF subunits are toxic, then

knockout of the subunit substrates should rescue the DCAF5-loss phenotype. To test this, we used the CRISPR-based competitive fitness assay to evaluate the knockout of three regulated subunits—*ARID1A*, *PBRM1* and *SMARCC1*—in RT cells. There was no selection against out-of-frame mutations in these subunits, either individually or collectively, in RT cells, suggesting that they have limited function in the absence of SMARCB1 (Extended Data Fig. 6a–c). CRISPR targeting of *DCAF5* alone resulted in a selection pressure against out-of-frame alleles, as before (Fig. 3e). However, the collective knockout of *ARID1A*, *PBRM1* and *SMARCC1* completely rescued the toxicity of *DCAF5* knockout, demonstrated by the lack of selection pressure against *DCAF5* out-of-frame alleles, as reflected by the maintenance of *DCAF5* knockout over time on the basis of western blotting (Fig. 3e and Extended Data Fig. 6d). Collectively, these results establish that accumulation of misassembled SWI/SNF complexes is the mechanism underlying dependency on DCAF5 in SMARCB1-deficient RT cells.

Article

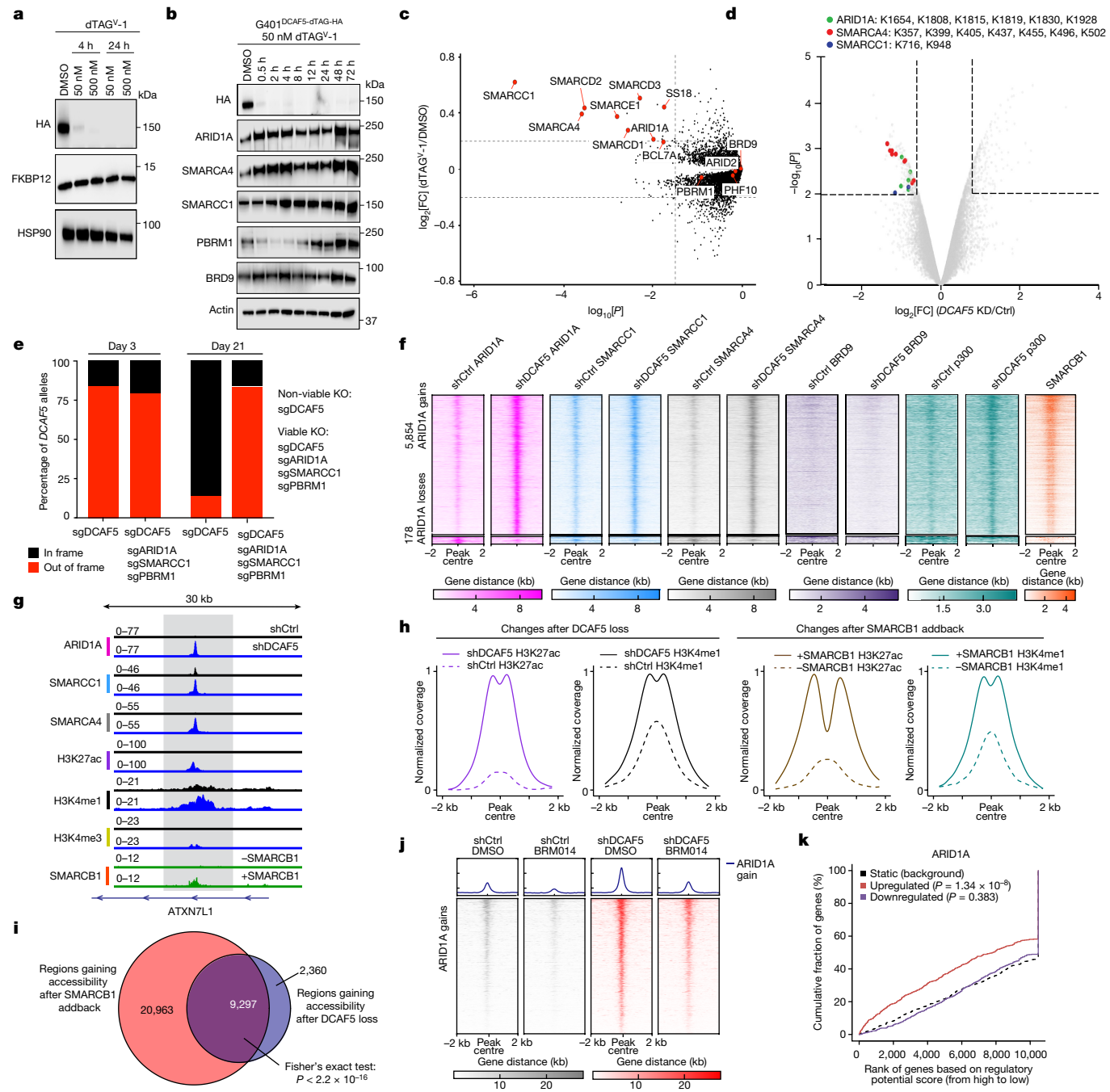


Fig. 3 | Inhibition of DCAF5 restores SWI/SNF function in SMARCB1-deficient cells. **a**, Western blot analysis of the G401-dTAG-DCAF5 pool after dTAGV-1 treatment. **b**, Western blot time course of G401-dTAG-DCAF5 clone E7 treated with dTAGV-1. **c**, Proteome analysis of G401-dTAG-DCAF5 cells after 24 h treatment with 50 nM dTAGV-1. Statistical analysis was performed using a moderated *t*-test in the limma package. The dashed lines indicate \log_2 -transformed fold change (FC) > 0.2 and $P < 0.05$. **d**, Ubiquitinome analysis of G401 cells with or without DCAF5 by di-Gly antibody enrichment and TMT quantification MS. Significance was assessed as described in **c**. The dashed lines indicate $\log_2[\text{FC}] > 0.68$ (-2 s.d.) and $P < 0.05$. **e**, Indel assay evaluating selection against DCAF5 out-of-frame alleles in BT16 SMARCB1-deficient RT cells with or without knockout (KO) of SWI/SNF subunits ARID1A, PBRM1 and SMARCC1. **f**, The effect of DCAF5 knockdown on ChIP-seq analysis of SWI/SNF subunits. Peak-centred heat maps within ± 2 kb of accessible regions for SWI/SNF subunits: ARID1A ($n = 3$ independent biological replicates), SMARCC1 ($n = 3$ independent biological replicates), SMARCA4 ($n = 2$ independent biological replicates), BRD9 ($n = 2$ independent biological replicates) and SMARCB1 ($n = 2$ independent biological replicates) along with p300 ($n = 3$ independent biological replicates). **g**, Sample locus in G401RT cells. **h**, The effect of DCAF5 knockdown on histone modifications ($n = 2$ independent biological replicates for each) at SWI/SNF target enhancers in RT cells (left). Right, comparison of changes after restoration of SMARCB1 ($n = 2$ independent biological replicates). **i**, Target genes that gain accessibility (ATAC-seq) after knockdown of DCAF5 compared to gain after SMARCB1 addback. Statistical analysis was performed using a one-sided Fisher's exact test; $P < 2.2 \times 10^{-16}$. **j**, Peak-centred heat maps within ± 2 kb of accessible regions gaining ARID1A (FC > 2, FDR < 0.05) with or without DCAF5 knockdown and with or without 1 μ M BRM014 inhibitor in G401 cells. **k**, Binding and Expression Target Analysis (BETA) comparing the gain of ARID1A binding after DCAF5 knockdown to changes in transcription. The red and blue lines represent activated and repressed genes, respectively, and the dashed line shows an unchanging gene set. Statistical analysis was performed using one-tailed Kolmogorov-Smirnov tests. Data are representative of two independent biological experiments (**a** and **b**). HA, haemagglutinin-tag.

independent biological replicates) at significant, differentially bound regions (FC > 2 and FDR < 0.05 for ARID1A) in G401 cells. **g**, Sample locus in G401RT cells. **h**, The effect of DCAF5 knockdown on histone modifications ($n = 2$ independent biological replicates for each) at SWI/SNF target enhancers in RT cells (left). Right, comparison of changes after restoration of SMARCB1 ($n = 2$ independent biological replicates). **i**, Target genes that gain accessibility (ATAC-seq) after knockdown of DCAF5 compared to gain after SMARCB1 addback. Statistical analysis was performed using a one-sided Fisher's exact test; $P < 2.2 \times 10^{-16}$. **j**, Peak-centred heat maps within ± 2 kb of accessible regions gaining ARID1A (FC > 2, FDR < 0.05) with or without DCAF5 knockdown and with or without 1 μ M BRM014 inhibitor in G401 cells. **k**, Binding and Expression Target Analysis (BETA) comparing the gain of ARID1A binding after DCAF5 knockdown to changes in transcription. The red and blue lines represent activated and repressed genes, respectively, and the dashed line shows an unchanging gene set. Statistical analysis was performed using one-tailed Kolmogorov-Smirnov tests. Data are representative of two independent biological experiments (**a** and **b**). HA, haemagglutinin-tag.

To understand why degradation of residual SWI/SNF complexes is essential for the proliferation of SMARCB1-deficient cancer cells, we first examined whether the SWI/SNF subunits that accumulate after DCAF5 inactivation bind to chromatin. We performed chromatin immunoprecipitation followed by sequencing (ChIP-seq) analysis of the SWI/SNF subunits SMARCA4, ARID1A, SMARCC1 and BRD9 and, to define enhancers and promoters, H3K27ac, H3K4me1 and H3K4me3 in G401 RT cells treated with shCtrl and shDCAF5.

After DCAF5 knockdown genomic binding of SMARCA4, ARID1A and SMARCC1 increased significantly (4,902, 5,854 and 5,129 gained sites, respectively) (Fig. 3f and Extended Data Fig. 7a–c). Co-occupancy analysis revealed extensive overlap of the sites gained by the three subunits, suggesting that cBAF and PBAF complexes (lacking SMARCB1) are binding to chromatin (Fig. 3f,g and Extended Data Fig. 7d,e). It is also possible that smaller subcomplexes or even monomers contribute to this binding and activity. Importantly, BRD9 (in the ncBAF complex) did not localize to these sites, either before or after DCAF5 loss, indicating that the gain of SMARCB1-deficient SWI/SNF complexes does not cause lethality by interfering with ncBAF function (Fig. 3f and Extended Data Fig. 7f–h). Using the dTAG system to identify early SWI/SNF targets after DCAF5 loss, we identified that 26% of these regions had gained SWI/SNF binding within 4 h of DCAF5 degradation (Extended Data Fig. 7i).

Given that the accumulated SMARCB1-deficient complexes are bound to chromatin, two possibilities emerged for the mechanism by which these complexes blocked the proliferation of the cancer cells. Either they lacked remodelling activity and interfered with functional components of the transcriptional regulatory machinery, or these SMARCB1-deficient complexes retained sufficient remodelling activity to rescue the cancer phenotype. To differentiate between these possibilities, we first examined whether the residual complexes lacking SMARCB1 that accumulate after DCAF5 loss bind to regions that are normally bound by wild-type SWI/SNF. We inducibly re-expressed SMARCB1 in G401 cells to define the normal SWI/SNF-binding landscape using CUT&RUN. The binding of SMARCA4, ARID1A and SMARCC1 after DCAF5 loss localized to sites to which wild-type SWI/SNF would normally bind (Fig. 3f and Extended Data Fig. 7g, h), indicating that inactivating DCAF5 rescued binding of the SMARCB1-deficient SWI/SNF complexes.

Given that SMARCB1 loss impairs enhancer function^{7,8,23,32}, we investigated the effect of the SMARCB1-deficient SWI/SNF complexes on the establishment of enhancers. After DCAF5 loss, binding of these complexes was predominantly gained at enhancers, with little binding at promoters (Extended Data Fig. 7j). SMARCB1 facilitates the establishment of H3K27ac and H3K4me1 at active enhancers²³. DCAF5 knockdown substantially rescued this effect in SMARCB1-deficient cells (Fig. 3h). Temporally, SWI/SNF binding preceded the gain of histone modifications (Extended Data Fig. 7i).

To elucidate the mechanism by which SMARCB1-deficient SWI/SNF complexes restore histone marks, we focused on the histone acetyltransferase p300 as we and others have previously demonstrated that SWI/SNF complexes directly bind to p300 and facilitate p300-mediated acetylation of H3K27^{6,8,33}. Furthermore, we have shown that the absence of SMARCB1 causes decreased protein levels of p300 in RT cells⁸. We found that DCAF5 loss leads to increased protein levels of p300 (Extended Data Fig. 7k) and co-localized binding with SWI/SNF at sites canonically bound by SMARCB1 (Fig. 3f and Extended Data Fig. 7l). Our data demonstrate that, after DCAF5 loss, SWI/SNF complexes are preferentially gained at lineage-specific enhancers and facilitate activity of p300 to modulate histone H3 lysine 27 acetylation, therefore restoring histone modifications that are otherwise lost in the absence of SMARCB1.

Next, we sought to understand whether SMARCB1-deficient SWI/SNF complexes retain their chromatin remodelling ability after the loss of DCAF5. Binding of residual SWI/SNF complexes was sufficient to significantly increase chromatin accessibility at 30% of the sites

that gained SWI/SNF-mediated accessibility after SMARCB1 addback, although not quite to the extent that occurred with re-expression of SMARCB1 (Fig. 3i and Extended Data Fig. 8a). To determine whether the accessibility gains were directly due to SWI/SNF activity, we used BRMO14, a small-molecule inhibitor that is specific for the SWI/SNF ATPases SMARCA4 and SMARCA2³⁴. After treatment with BRMO14 for 2 h, the effect of DCAF5 knockdown was nearly completely rescued, as measured using the assay for transposase-accessible chromatin with sequencing (ATAC-seq; Fig. 3j). This indicates that chromatin remodelling by SWI/SNF is still possible without SMARCB1, at least to some extent. Although perhaps surprising given the interpretation of recent structural models³⁵, this finding is consistent with previous studies that showed that the SMARCA4 ATPase alone is capable of remodelling mononucleosomes and nucleosomal arrays, with the addition of SMARCB1, SMARCC1 and SMARCC2 stimulating activity³⁶.

AP-1 sites have previously been reported by us and others to be the most enriched transcription factor motifs at sites of SWI/SNF activity^{8,37,38}. Consequently, we assessed the transcription factor motifs at SWI/SNF-gained/ATAC-gained sites in shDCAF5 cells and compared them with motifs at gained sites in SMARCB1 re-expressed cells. AP-1 and TEAD4 were the top two motifs gained in both conditions (Extended Data Fig. 8b,c). Similarly, while minimal changes in chromatin accessibility were observed 4 h after DCAF5 degradation, there was marked enrichment for AP-1 and TEAD4 transcription factors at 1,527 regions with early accumulation of SWI/SNF (Extended Data Fig. 8d,e). Thus, DCAF5 inactivation in SMARCB1-deficient cancer cells is sufficient to restore the binding of residual SWI/SNF complexes at their normal sites, facilitate the acquisition of active enhancer-specific covalent histone modifications and restore chromatin accessibility at a substantial number of these sites.

We next evaluated how binding of residual SWI/SNF complexes affected gene expression in the absence of DCAF5. The binding of ARID1A, SMARCC1 and SMARCA4 was each significantly associated with genes upregulated after DCAF5 loss (Fig. 3k and Extended Data Fig. 8f,g). Approximately 90% of the SMARCC1, ARID1A and SMARCA4 upregulated target genes after DCAF5 knockdown shared binding of all three subunits (Extended Data Fig. 8h). We compared genes activated by DCAF5 loss to those that were differentially expressed after re-expression of SMARCB1 and found a highly significant positive correlation (Extended Data Fig. 8i). Furthermore, Gene Ontology analysis revealed that genes upregulated by DCAF5 inhibition were significantly enriched in developmental processes and have a high degree of overlap with pathways upregulated after SMARCB1 re-expression²³ (Extended Data Fig. 8i,j). Collectively, these data demonstrate that the lethality mediated by DCAF5 inactivation occurs due to residual SWI/SNF complexes substantially rescuing the transcriptional consequences of SMARCB1 loss, thereby reversing the cancer state through restoration of differentiation pathways.

As β-propeller family proteins have been demonstrated to be therapeutically targetable^{39–42}, we evaluated the consequences of DCAF5 loss after RT growth in vivo. We injected G401-dTAG-DCAF5 cells expressing YFP-luciferase into athymic nude mice, which were randomized and enrolled in the study if they met predetermined criteria (Fig. 4a and Extended Data Fig. 9a–d). The preplanned treatment regimen consisted of two 3-week courses during which dTAG^{V-1} was administered for 5 consecutive days during weeks 1 and 2, then withheld on week 3 (Fig. 4b). The response to degradation of DCAF5 by dTAG^{V-1} was rapid and marked, meeting predefined criteria for a complete response⁴³ (Fig. 4c,d). Given the potential therapeutic relevance of targeting DCAF5, we sought to evaluate toxicity in normal cells, including during development. We therefore generated germline *Dcaf5*-knockout mice. Germline *Dcaf5*-knockout mice were viable and indistinguishable from littermate controls at least until the most recent timepoint of 12 weeks of age (Fig. 4e–g, Extended Data Fig. 9e and Supplementary Video 1).

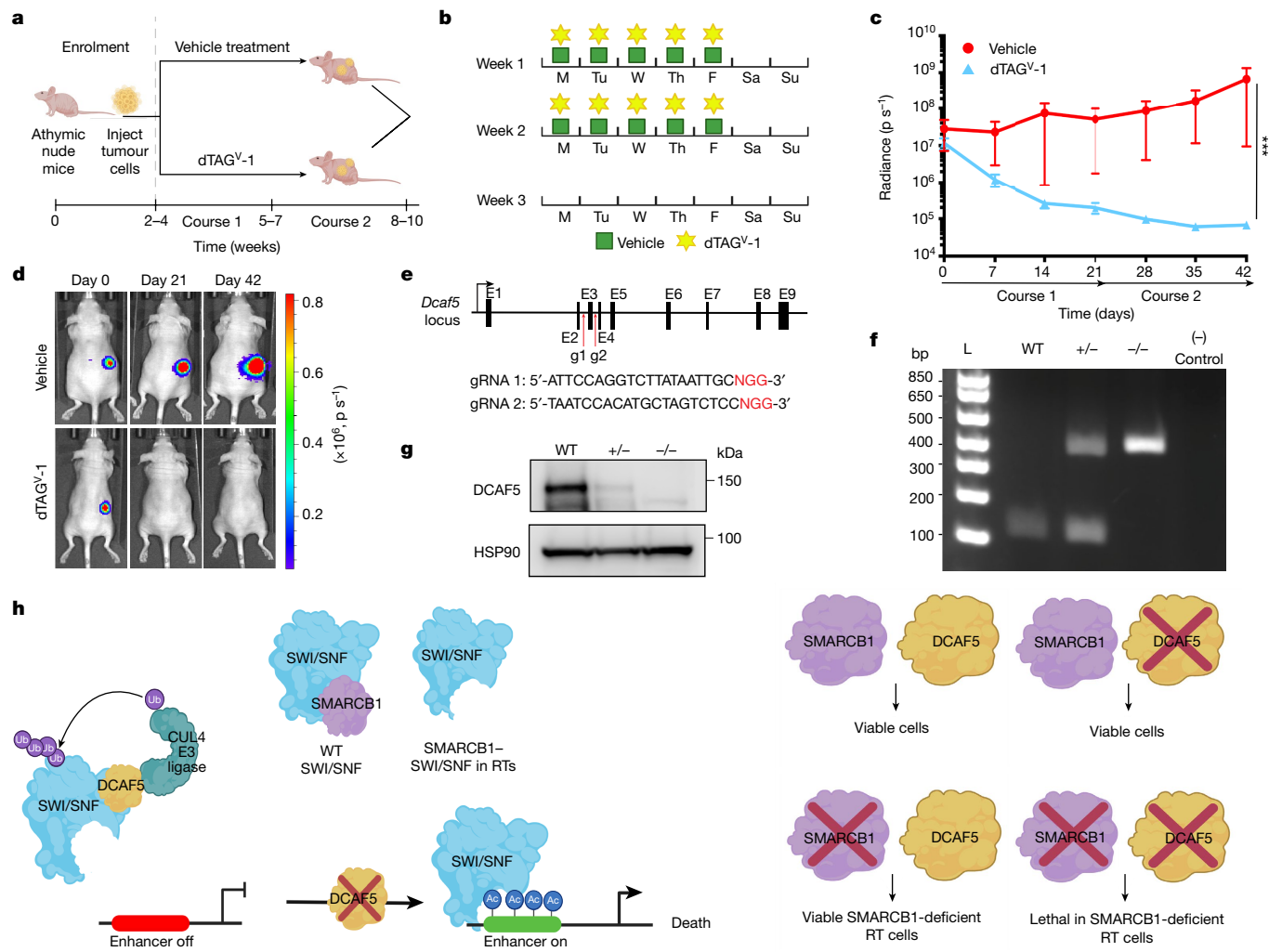


Fig. 4 | DCAF5 is a therapeutically tractable target in vivo. **a**, Schematic of the in vivo study design. **b**, The dosing schedule for dTAG^{V-1} in course 1 and course 2. **c**, In vivo mouse bioluminescence imaging. Data are mean \pm s.e.m. radiance (photons s⁻¹) over time (days) of animals treated with vehicle (red) or dTAG^{V-1} (blue). $n = 10$ mice per treatment group. Statistical analysis was performed using two-way analysis of variance; *** $P = 0.0001$. **d**, Representative bioluminescence images of vehicle and dTAG^{V-1} mice at day 0, day 21 and day 42. **e**, The strategy to delete mouse *Dcaf5*. **f**, Representative genotyping of germline *Dcaf5*-knockout mice by PCR. $n = 11$ mice per genotype. L, DNA ladder size markers; WT, wild type. **g**, Western blot analysis of kidney tissue extracts from

WT, heterozygous (+/−) and homozygous (−/−) germline *Dcaf5*-knockout mice. The experiment was performed once. **h**, Model of the mechanism of DCAF5 loss in RTs. DCAF5 has a quality-control function for SWI/SNF complexes. The loss of the SMARCB1 tumour suppressor triggers DCAF5 to degrade the residual SWI/SNF complex members. Targeted inactivation of DCAF5 rescues substantial SWI/SNF function, resulting in the restoration of active histone modifications at enhancers accompanied by restoration of SWI/SNF-mediated gene expression. This reverses the cancer phenotype by restoring differentiation. The diagrams in **a**, **b** and **h** were created using BioRender.

Discussion

Conceptually, targeting synthetic lethal relationships offers great promise for the treatment of tumour-suppressor-driven cancers. However, objective identification of synthetic lethal relationships in cancer has often proven to be challenging given the large number of genes that must be evaluated and the consequent signal-to-noise challenges when assessing a limited number of models. The advent of near genome-wide CRISPR vulnerability screens in many hundreds of cell lines, such as DepMap, offers the potential to reveal vulnerabilities that are robust and highly specific, as is the case with our finding that the little-studied DCAF5 is a targetable vulnerability in SMARCB1-deficient cancer cells.

The mechanism underlying synthetic lethal relationships is frequently unclear. However, when identified, it often relies on creating a toxicity to which the mutant cancer cells are somewhat more sensitive than normal cells. For example, PARP inhibition causes DNA strand breaks that BRCA-mutant cells are defective in repairing, therefore

creating greater toxicity in the cancer cells than in the patient's normal cells⁴⁴. Similarly, inactivating the sole remaining SWI/SNF complex family (ncBAF) in SMARCB1-mutant cells creates preferential toxicity^{20,25,45}.

Here we identified a synthetic lethal relationship that functions differently. Rather than creating a toxicity, targeted inactivation of a quality-control factor substantially restores the function of a multi-subunit protein complex that is otherwise degraded after the loss of a tumour suppressor subunit. We and others have previously demonstrated that SMARCB1 loss drives cancer by impairing the activation of enhancers in highly proliferative progenitor cells, therefore blocking differentiation and enabling continued proliferation^{7,8,32}. Mechanistically, the inactivation of DCAF5 rescues substantial SWI/SNF function, restores differentiation and reverses the cancer phenotype (Fig. 4h).

Previously, ubiquitin-dependent pathways, including cullin-RING ubiquitin ligase family proteins, have been implicated in the quality control of multiprotein complexes⁴⁶. This includes roles in aberrant complex formation, such as the E3 ligase SCF-FBXL17⁴⁷. SMARCB1-mutant

cancers have been reported to show enhanced sensitivity to global proteasome inhibition, but the mechanism is unclear⁴⁸. We show that DCAF5 has a quality-control function for SWI/SNF complexes through promoting the degradation of SWI/SNF subunits in the absence of SMARCB1. We previously demonstrated that SMARCB1 loss causes greater destabilization of SWI/SNF complexes than the loss of SMARCA4 or ARID1A, likely explaining the preferential dependence of SMARCB1-mutant cancers compared with other SWI/SNF mutant cancers on DCAF5^{23,49,50}.

This synthetic lethal relationship suggests potential therapeutic routes as recent studies have demonstrated that β-propeller proteins such as DCAF5 are readily druggable³⁹. Two examples include WDR5 and EED, the latter of which is in clinical trials for diffuse large B cell lymphoma^{40–42,51}. Our demonstration that the degradation of DCAF5 is sufficient to eliminate SMARCB1-deficient tumours in vivo combined with our finding that *Dcaf5* is dispensable for the development and viability of mice suggests DCAF5 as a compelling therapeutic target. Our cryo-EM structure of DCAF5 will facilitate the development of inhibitors/degraders and therapeutic translation for these highly lethal cancers.

Collectively, our data reveal a mechanism that underlies the quality control of a multiprotein complex and constitutes a targetable synthetic lethal vulnerability in cancers driven by mutational inactivation of a tumour suppressor.

Online content

Any methods, additional references, Nature Portfolio reporting summaries, source data, extended data, supplementary information, acknowledgements, peer review information; details of author contributions and competing interests; and statements of data and code availability are available at <https://doi.org/10.1038/s41586-024-07250-1>.

1. Dharia, N. V. et al. A first-generation pediatric cancer dependency map. *Nat. Genet.* **53**, 529–538 (2021).
2. Doench, J. G. et al. Optimized sgRNA design to maximize activity and minimize off-target effects of CRISPR-Cas9. *Nat. Biotechnol.* **34**, 184–191 (2016).
3. Meyers, R. M. et al. Computational correction of copy number effect improves specificity of CRISPR-Cas9 essentiality screens in cancer cells. *Nat. Genet.* **49**, 1779–1784 (2017).
4. Mittal, P. & Roberts, C. W. M. The SWI/SNF complex in cancer—biology, biomarkers and therapy. *Nat. Rev. Clin. Oncol.* **17**, 435–448 (2020).
5. Zhu, Z. et al. Mitotic bookmarking by SWI/SNF subunits. *Nature* **618**, 180–187 (2023).
6. Wang, X. et al. SMARCB1-mediated SWI/SNF complex function is essential for enhancer regulation. *Nat. Genet.* **49**, 289–295 (2017).
7. Nakayama, R. T. et al. SMARCB1 is required for widespread BAF complex-mediated activation of enhancers and bivalent promoters. *Nat. Genet.* **49**, 1613–1623 (2017).
8. Alver, B. H. et al. The SWI/SNF chromatin remodelling complex is required for maintenance of lineage specific enhancers. *Nat. Commun.* **8**, 14648 (2017).
9. Valencia, A. M. et al. Recurrent SMARCB1 mutations reveal a nucleosome acidic patch interaction site that potentiates mSWI/SNF complex chromatin remodeling. *Cell* **179**, 1342–1356 (2019).
10. Verstege, I. et al. Truncating mutations of hSNF5/INI1 in aggressive paediatric cancer. *Nature* **394**, 203–206 (1998).
11. Lee, R. S. et al. A remarkably simple genome underlies highly malignant pediatric rhabdoid cancers. *J. Clin. Invest.* **122**, 2983–2988 (2012).
12. Le Roarer, F. et al. Consistent SMARCB1 homozygous deletions in epithelioid sarcoma and in a subset of myoepithelial carcinomas can be reliably detected by FISH in archival material. *Genes Chromosomes Cancer* **53**, 475–486 (2014).
13. Roberts, C. W. M., Leroux, M. M., Fleming, M. D. & Orkin, S. H. Highly penetrant, rapid tumorigenesis through conditional inversion of the tumor suppressor gene *Snf5*. *Cancer Cell* **2**, 415–425 (2002).
14. Leng, F. et al. Methylated DNMT1 and E2F1 are targeted for proteolysis by L3MBTL3 and CRL4^{DCAF5} ubiquitin ligase. *Nat. Commun.* **9**, 1641 (2018).
15. Zhang, C. X. et al. Proteolysis of methylated SOX2 protein is regulated by L3MBTL3 and CRL4^{DCAF5} ubiquitin ligase. *J. Biol. Chem.* **294**, 476–489 (2019).
16. He, Y. Z. J., McCall, C. M., Hu, J., Zeng, Y. X. & Xiong, Y. DDB1 functions as a linker to recruit receptor WD40 proteins to CUL4-ROC1 ubiquitin ligases. *Genes Dev.* **20**, 2949–2954 (2006).
17. Lee, J. & Zhou, P. DCAF5s, the missing link of the CUL4-DDB1 ubiquitin ligase. *Mol. Cell* **26**, 775–780 (2007).
18. Ahn, J. et al. The cullin-RING E3 ubiquitin ligase CRL4-DCAF1 complex dimerizes via a short helical region in DCAF1. *Biochemistry* **50**, 1359–1367 (2011).
19. Angers, S. et al. Molecular architecture and assembly of the DDB1-CUL4A ubiquitin ligase machinery. *Nature* **443**, 590–593 (2006).
20. Wang, X. et al. BRD9 defines a SWI/SNF sub-complex and constitutes a specific vulnerability in malignant rhabdoid tumors. *Nat. Commun.* **10**, 1881 (2019).
21. Shabek, N. et al. Structural insights into DDA1 function as a core component of the CRL4-DDB1 ubiquitin ligase. *Cell Discov.* **4**, 67 (2018).
22. Li, T., Robert, E. I., van Breugel, P. C., Strubin, M. & Zheng, N. A promiscuous α-helical motif anchors viral hijackers and substrate receptors to the CUL4-DDB1 ubiquitin ligase machinery. *Nat. Struct. Mol. Biol.* **17**, 105–111 (2010).
23. Wang, X. F. et al. SMARCB1-mediated SWI/SNF complex function is essential for enhancer regulation. *Cancer. Res.* <https://doi.org/10.1158/1538-7445.Am2017-Lb-096> (2017).
24. Alpsoy, A. & Dykhuizen, E. C. Glioma tumor suppressor candidate region gene 1 (GLTSCR1) and its paralog GLTSCR1-like form SWI/SNF chromatin remodeling subcomplexes. *J. Biol. Chem.* **293**, 3892–3903 (2018).
25. Michel, B. C. et al. A non-canonical SWI/SNF complex is a synthetic lethal target in cancers driven by BAF complex perturbation. *Nat. Cell Biol.* **20**, 1410–1420 (2018).
26. Guo, P. et al. The assembly of mammalian SWI/SNF chromatin remodeling complexes is regulated by lysine-methylation dependent proteolysis. *Nat. Commun.* **13**, 6696 (2022).
27. Nabet, B. et al. Rapid and direct control of target protein levels with VHL-recruiting dTAG molecules. *Nat. Commun.* **11**, 4687 (2020).
28. Nabet, B. et al. The dTAG system for immediate and target-specific protein degradation. *Nat. Chem. Biol.* **14**, 431–441 (2018).
29. Mashalir, N. et al. Modular organization and assembly of SWI/SNF family chromatin remodeling complexes. *Cell* **175**, 1272–1288 (2018).
30. Evans, R. et al. Protein complex prediction with AlphaFold-Multimer. Preprint at *bioRxiv* <https://doi.org/10.1101/2021.10.04.463034> (2022).
31. Peng, J. et al. A proteomics approach to understanding protein ubiquitination. *Nat. Biotechnol.* **21**, 921–926 (2003).
32. Langer, L. F., Ward, J. M. & Archer, T. K. Tumor suppressor SMARCB1 suppresses super-enhancers to govern hESC lineage determination. *eLife* **8**, e45672 (2019).
33. Huang, Z. Q., Li, J., Sachs, L. M., Cole, P. A. & Wong, J. A role for cofactor-cofactor and cofactor-histone interactions in targeting p300, SWI/SNF and Mediator for transcription. *EMBO J.* **22**, 2146–2155 (2003).
34. Schick, S. et al. Acute BAF perturbation causes immediate changes in chromatin accessibility. *Nat. Genet.* **53**, 269–278 (2021).
35. Mashalir, N. et al. A structural model of the endogenous human BAF complex informs disease mechanisms. *Cell* **183**, 802–817 (2020).
36. Phelan, M. L., Sif, S., Narlikar, G. J. & Kingston, R. E. Reconstitution of a core chromatin remodeling complex from SWI/SNF subunits. *Mol. Cell* **3**, 247–253 (1999).
37. Wolf, B. K. et al. Cooperation of chromatin remodeling SWI/SNF complex and pioneer factor AP-1 shapes 3D enhancer landscapes. *Nat. Struct. Mol. Biol.* **30**, 10–21 (2023).
38. Vierbuchen, T. et al. AP-1 transcription factors and the BAF complex mediate signal-dependent enhancer selection. *Mol. Cell* **68**, 1067–1082 (2017).
39. Schapira, M., Tyers, M., Torrent, M. & Arrowsmith, C. H. WD40 repeat domain proteins: a novel target class? *Nat. Rev. Drug Discov.* **16**, 773–786 (2017).
40. Grebien, F. et al. Pharmacological targeting of the Wdr5–MLL interaction in C/EBPα N-terminal leukemia. *Nat. Chem. Biol.* **11**, 571–578 (2015).
41. He, Y. P. et al. The EED protein-protein interaction inhibitor A-395 inactivates the PRC2 complex. *Nat. Chem. Biol.* **13**, 922–922 (2017).
42. Qi, W. et al. An allosteric PRC2 inhibitor targeting the H3K27me3 binding pocket of EED. *Cancer Res.* <https://doi.org/10.1158/1538-7445.Am2017-Lb-288> (2017).
43. Stewart, E. et al. Targeting the DNA repair pathway in Ewing sarcoma. *Cell Rep.* **9**, 829–840 (2014).
44. Lord, C. J. & Ashworth, A. PARP inhibitors: Synthetic lethality in the clinic. *Science* **355**, 1152–1158 (2017).
45. Brien, G. L. et al. Targeted degradation of BRD9 reverses oncogenic gene expression in synovial sarcoma. *eLife* **7**, e41305 (2018).
46. Padovani, C., Jevtic, P. & Rape, M. Quality control of protein complex composition. *Mol. Cell* **82**, 1439–1450 (2022).
47. Mena, E. L. et al. Dimerization quality control ensures neuronal development and survival. *Science* **362**, eaap8236 (2018).
48. Hong, A. L. et al. Renal medullary carcinomas depend upon SMARCB1 loss and are sensitive to proteasome inhibition. *eLife* **8**, e44161 (2019).
49. Helming, K. C. et al. ARID1B is a specific vulnerability in ARID1A-mutant cancers. *Nat. Med.* **20**, 251–254 (2014).
50. Wilson, B. G. et al. Residual complexes containing SMARCA2 (BRM) underlie the oncogenic drive of SMARCA4 (BRG1) mutation. *Mol. Cell. Biol.* **34**, 1136–1144 (2014).
51. Wang, L., Li, L. R. & Young, K. H. New agents and regimens for diffuse large B cell lymphoma. *J. Hematol. Oncol.* **13**, 175 (2020).

Publisher's note Springer Nature remains neutral with regard to jurisdictional claims in published maps and institutional affiliations.

Springer Nature or its licensor (e.g. a society or other partner) holds exclusive rights to this article under a publishing agreement with the author(s) or other rightsholder(s); author self-archiving of the accepted manuscript version of this article is solely governed by the terms of such publishing agreement and applicable law.

© The Author(s), under exclusive licence to Springer Nature Limited 2024, corrected publication 2024

Article

Methods

Cell culture

G401(ATCC-CRL1441), G402(ATCC-CRL-1440), HCT116(ATCC-CCL-247), MCF7(ATCC HTB-22) and HEK293T(ATCC-CRL-3216) cell lines were purchased from ATCC. TTC549 cells were obtained through a material transfer agreement from T. Triche. MON cells were obtained through a material transfer agreement from F. Bourdeaut. BT16 cells were obtained through a material transfer agreement from C.D.James. CH22 cells were a gift from The Chordoma Foundation and B. E. Weissman. TTC549, MON, BT16 and CH22 cells were obtained through a material transfer agreement. G401, G402 and HCT116 cells were cultured in McCoy's medium with 10% FBS (Sigma-Aldrich) and 1% GlutaMAX (GIBCO). MON and TTC549 cells were cultured in RPMI medium with 10% FBS and 1% GlutaMAX. BT16, HEK293T and MCF7 cells were cultured in DMEM medium with 10% FBS and 1% GlutaMAX. CH22 cells were cultured in a 4:1 ratio of IMDM:RPMI with 20% FBS and 10% 100× MEM NEAA (GIBCO). All cells were cultured at 37 °C with 95% humidity and under 5% CO₂ and were regularly tested for mycoplasma by PCR (Genlantis). Cells were transduced at a multiplicity of infection of 10 with shRNAs in the presence of Polybrene (8 µg ml⁻¹, Santa Cruz) and selected for 72 h with 1 µg ml⁻¹ puromycin (Thermo Fisher Scientific). Tet-inducible SMARCB1RT cells²⁰ were maintained in Tet-system approved FBS and induced with doxycycline (1 µg ml⁻¹, Clontech) for the indicated time.

Generation of dTAG Lines

G401 and BT16 cells were co-infected with FKBP12(F36V)-2×HA-tagged DCAF5 and sgRNAs targeting *DCAF5* to replace endogenous DCAF5 with FKBP12(F36V)-2×HA-tagged DCAF5. Cells were selected with both 1 µg ml⁻¹ puromycin (FKBP12(F36V)-2×HA-tagged DCAF5) and 1 µg ml⁻¹ blasticidin (sgRNA). pLEX_305-DCAF5-dTAG was generated as previously described²⁷. dTAG^{V-1} was synthesized as previously described²⁷. Pooled cells were sorted into single-cell clones using the Aria cell sorter (BD Biosciences) by the Flow Cytometry and Cell Sorting Shared Resource at St Jude Children's Research Hospital. Clones were subjected to confirmatory deep targeted sequencing by the Center for Advanced Genomic Engineering at St Jude Children's Research Hospital. G401 DCAF5-dTAG cells were prepared for in vivo studies by infection with YFP-tagged luciferase lentivirus and selected in puromycin (1 µg µl⁻¹) for 72 h. YFP-positive cells were sorted using the Aria cell sorter (BD Biosciences).

In vivo xenograft studies

Athymic nude immunodeficient mice were purchased from Charles River (strain code, 553; stress level, C). Mice were aged 6–12 weeks and the sample size was chosen on the basis of a power analysis. Mice were subcutaneously implanted with 1.5 × 10⁶ G401 DCAF5-dTAG-YFP-luciferase cells. Tumour growth was measured weekly by IVIS bioluminescence. Mice were weighed at least weekly. The mice were randomized and enrolled into treatment arms using a blocked randomization list (<https://www.sealedenvelope.com/simple-randomiser/v1/lists>) when animals met enrolment criteria of either visible tumour or a luminescence reading of 10⁷ photons s⁻¹. After randomization, no blinding was performed. Animals were considered to be moribund when tumours reached 2 cm in any one dimension or reached humane end points. Disease response was classified based on bioluminescence signal, as previously described³². Animals were housed under a 12 h–12 h light–dark cycle (light on at 06:00 and off at 18:00) and food and water were provided ad libitum. Animals are housed in the facility at 68–70 F (20–22 °C) with humidity levels maintained at 30–70% at cage level. Animal maintenance and procedures were performed in accordance with the National Institutes of Health Guide for the Care and Use of Laboratory Animals. The animal protocol was approved by the Institutional Animal Care and Use Committee at St Jude Children's Research Hospital. All efforts were made to minimize suffering.

Xenogen imaging and quantification

Mice bearing G401 DCAF5-dTAG-YFP-luciferase cells were injected intraperitoneally with firefly d-luciferin (Caliper Life Sciences; 3 mg per mouse). Bioluminescence images were taken 5 min later luciferase injection using the IVIS 200 imaging system. Anaesthesia was administered throughout image acquisition (isoflurane 1.5% in O₂ at 2 l min⁻¹). The Living Image v.4.3 software (Caliper Life Sciences) was used to generate a standard region of interest (ROI) encompassing the largest tumour at the maximal bioluminescence signal. The identical ROI was used to determine the average radiance (photons s⁻¹) for all xenografts.

In vivo compound formulation

For IP injections, dTAG^{V-1} was dissolved in DMSO and then diluted with 20% solutol (Sigma-Aldrich): 0.9% sterile saline (Moltox) (w/v) with the final formulation containing 5% DMSO. Mice were dosed with 40 mg per kg of dTAG^{V-1} on Monday to Friday week 1 and 2 and were not dosed on week 3.

Generation of the germline *Dcaf5*-knockout model

Generating the germline *Dcaf5*-knockout model was performed under the guidelines of the St Jude Children's Research Hospital IACUC. Male and female C57Bl/6 mice (aged 6 weeks) were purchased from Jackson Laboratory (000664). Animal care was facilitated by the Animal Husbandry Unit at St Jude Children's Research Hospital in accordance with their guidelines and regulations. The germline *Dcaf5*-knockout mouse model was created using CRISPR–Cas9 technology and direct zygote injection as previously described³³. sgRNAs targeting *Dcaf5* were generated by the Center of Advanced Genome Engineering at St Jude Children's Research Hospital. An analysis was performed for sgRNA validation and minimization of off-target deletions in the mouse genome.

Four separate nucleofections were performed in N2A-Cas9 cells using the following combinations: 5' g11 + sense ssODNs; 5' g11 + antisense ssODNs; 3' g21 + sense ssODNs; 3' guide (g21) with antisense ssODNs for optimal integration analysis.

A mixture of the two sgRNAs for the 5' and 3' (10 ng µl⁻¹ each) and SpCas9 (40 ng µl⁻¹) was injected into the pronucleus of C57BL/6 fertilized oocytes to delete exon 3, resulting in a premature stop codon in exon 4. The resulting pups were genotyped using PCR and gel electrophoresis. At 6 weeks of age, the mice were backcrossed to C57BL/6 mice and bred to homozygosity. The deletion was confirmed by Sanger sequencing, and knockout was confirmed by PCR and western blotting. A list of the relevant genome-editing reagents and primers is provided in Supplementary Table 10.

Genotyping

Genomic DNA from tail biopsies of postnatal day 11–21 (P11–21) mice was extracted using 200 µl of 50 nM NaOH and Tris-HCl (pH 8). PCR amplification was achieved using the Promega GoTaq Green Master Mix (M7122) using the primers (Integrated DNA Technologies) listed in Supplementary Table 3.

The resulting PCR product was analysed by rapid gel electrophoresis (Invitrogen E-Gel Agarose Gels with SYBR Safe DNA Gel Stain, 2%).

Vectors and stable cell line generation

DCAF5 knockdown was achieved by lentiviral infection (multiplicity of infection = 10) with CMV-driven PLKO Mission shRNA TRCN0000425851 (TGTTAACCAAGTCCGATTAA) and TRCN0000146480 (CCCAAAT TTGATGGCACATT) and selected with 1 µg ml⁻¹ puromycin (GIBCO) for 72 h. *L3MBTL3* and *KDM1A* knockdown were achieved similarly using Mission shRNAs TRCN0000431896 (CAATCGTTCTGGT ACATT), TRCN0000046072 (CCACGAGTCAAACCTTTATT) and TRCN0000046068 (GCCTAGACATTAAACTGAATA). The non-targeting control TRC2 PLKO Mission scramble shRNA SHC202 was used. Isogenic SMARCB1-knockout HEK293T cells were generated as

described previously²⁰. Inducible cells were then subjected to subsequent infection with either shDCAF5 or non-targeting control followed by selection in puromycin ($1\mu\text{g ml}^{-1}$) for 72 h and simultaneous induction of SMARCB1 or GFP 72 h.

Lentiviral generation and infection

The production and titration of lentiviral vectors was performed as described previously⁵⁴ and vectors were generated by the St Jude Vector Production and Development Core. The detailed protocol is provided in the Supplementary Information.

Anti-hDCAF5 polyclonal antibody generation

The DNASTar Protean program was used to predict antigenic peptides within DCAF5 for immunization of rabbits to generate polyclonal antibody sera. A prominent region highlighted by the hydrophilicity plot (Kyte-Doolittle), antigenic index (Jameson-Wolf) and surface probability plot (Emini) was selected. Two peptides (S65–585, EDEELNERRAST-WQRN; and 586–600, AMRRRQKTTREDKPS) were generated in house (St Jude Peptide Synthesis Core) to span this region. Both peptides were coupled to keyhole limpet haemocyanin (KLH) and sent to Cocalico Biologicals for immunization of rabbits. After a prime, boost and boost regimen, test bleeds (2 weeks after the last boost) were provided for testing. The sera were tested by enzyme-linked immunosorbent assay, using peptide-coated (not coupled to KLH) plates, SDS-PAGE/western blotting and IP from cell lysate for screening. The most optimal rabbits were then selected on the basis of these results for a final boost and terminal bleed. Cocalico Biologicals affinity purified peptide specific antibodies from the sera.

Cell viability and proliferation assays

Cells were transduced with shDCAF5 or shCtrl at a multiplicity of infection of 10 for 48 h and were subjected to puromycin selection ($1\text{--}2\mu\text{g ml}^{-1}$). After selection, cells were seeded into 96-well plates. Cell proliferation was recorded using the IncuCyte live-cell imaging system (Essen Bioscience) according to the manufacturer's recommendations. The recorded cell confluence data were analysed by IncuCyte Zoom software and plotted using GraphPad Prism 9.

ChIP analysis

ChIP experiments were performed as previously described⁵. A total of 5 µg of the following antibodies was used: SMARCC1 (Thermo Fisher Scientific, PA5-30174), BRG1 (Abcam, ab110641), ARID1A (Sigma-Aldrich, HPA005456), PBRM1 (Bethyl, A700-019), BRD9 (CST, 58906), p300 (ab10485), H3K27ac (ab4729), H3K4me3 (ab8580) and H3K4me1 (ab8895). The KAPA Hyper Prep Kit (KK8504) was used for library preparation before sequencing. Library concentration and size distribution were assessed using the Agilent TapeStation and D1000 high-sensitivity Screenshot. Next-generation sequencing was performed at the Hartwell Genome Sequencing Facility at St Jude Children's Research Hospital using the NovaSeq 6000 (Illumina) system to generate 50 bp single-end reads.

CUT&RUN

CUT&RUN was performed as previously described⁵⁵. For each sample, 0.5×10^6 cells were used. A total of 1 µl SMARCB1 (Cell Signaling Technologies, 91735) was incubated with bead-bound, permeabilized cells overnight. The KAPA Hyper Prep Kit (KK8504) was used for library preparation. Library concentration and size distribution were assessed using the Agilent TapeStation and D1000 high-sensitivity Screenshot. Paired-end 75 bp sequencing was performed on libraries using the NovaSeq 6000 sequencer.

ATAC-seq

ATAC-seq experiments were performed on 100,000 G401 shCtrl or shDCAF5 cells treated with DMSO or BRM014 (HY-119374, MedChem-Express) at a final concentration of 1 µM or dTAG-DCAF5 cells treated

with 50 nM of dTAGV-1 or DMSO for 4 h according to manufacturer guidelines (Active Motif, 53150). Libraries were generated using purified DNA, according to manufacturer guidelines. At least 50×10^6 , 100 bp, paired-end reads were generated on the Illumina NovaSeq 6000 system.

Whole-cell protein extraction

Cells were lysed in NP-40 lysis buffer (150 mM NaCl, 0.5% NP-40, 50 mM Tris-HCl pH 8.0) with 1× protease and phosphatase inhibitors for 30 min on ice and were subsequently centrifuged at 13,000 rpm for 10 min. Protein was quantified using the Bradford assay (Bio-Rad).

IP analysis

A total of 0.5–1 mg of whole-cell extract was incubated either with 5 µg of antibody of interest or rabbit IgG antibody (Cell Signaling Technology) while rotating at 4 °C for 16 h. The beads were then separated on a magnet and washed three times with NP-40 lysis buffer (150 mM NaCl, 0.5% NP-40, 50 mM Tris-HCl pH 8.0). Protein was eluted from beads using 1× LDS buffer containing 10% 2-mercaptoethanol at 70 °C for 10 min.

Cycloheximide pulse experiments

G401 shCtrl- and shDCAF5-treated cells were pulsed with 50 µg ml⁻¹ cycloheximide (C7698-5G) for 0 to 24 h and collected for western blot analysis.

Glycerol gradient fractionation

Nuclear fractions were extracted from RT cells⁵. A total of 1 mg of nuclear protein from each cell line was added to a 15 ml 10–30% glycerol gradient and centrifuged in an SW40 rotor for 16 h at 40,000 rpm at 4 °C. The fractions were collected, processed for gel electrophoresis and analysed using western blotting.

Immunoblotting

A total of 25 µg of protein from cell lysates or 100 µg of mouse tissue lysate was electrophoresed on either NuPAGE 4–12% Bis-Tris or NuPAGE 3–8% Tris-acetate gels (Invitrogen). Western blotting was performed as previously described⁵. Blots were imaged using the LI-COR Odyssey Fc system and the LI-COR Image Studio software (LI-COR Biosciences, v.5.5.4). A list of antibodies and dilutions is provided in Supplementary Table 9. Immunoblot source data are provided in Supplementary Fig. 1.

DCAF5 CRISPR–Cas9 indel fitness assays

A total of 1×10^6 cells was transiently transfected with designed guides or non-targeting control guides (Supplementary Table 11). Guides were delivered as a precomplexed ribonuclear protein consisting of 150 pmol of chemically modified sgRNA (Synthego) and 50 pmol of Cas9 protein (St Jude Protein Production Facility) by nucleofection (Lonza, 4D-Nucleofector X-unit) using solution P3 and program EH-100 in a small (20 µl) cuvette according to the manufacturer's recommended protocol. A portion of cells was collected for gDNA at 7, 14 and 21 days after nucleofection. Genomic DNA was sequenced by targeted deep sequencing using gene specific primers with partial Illumina adapter overhangs (Supplementary Table 11). Next-generation sequencing analysis of edited cell pools was performed using CRIS.py⁵⁶. All indels were binned into in-frame, out-of-frame or 0 bp indels.

RNA-seq analysis

RNA from G401 RT cells was extracted using Trizol (Invitrogen) and the DirectZol Miniprep Plus Kit (Zymo Research, R2070). RNA was quantified using the Quant-iT RiboGreen RNA assay (Thermo Fisher Scientific) and the quality was checked using the 2100 Bioanalyzer RNA 6000 Nano assay (Agilent) or the 4200 TapeStation RNA Screen-Tape assay (Agilent). Libraries were prepared from total RNA using

Article

the TruSeq Stranded mRNA Library Prep Kit according to the manufacturer's instructions (Illumina, 20020595). Libraries were analysed for insert size distribution using the 2100 BioAnalyzer High Sensitivity kit (Agilent), 4200 TapeStation D1000 ScreenTape assay (Agilent) or 5300 Fragment Analyzer NGS fragment kit (Agilent). Libraries were quantified using the Quant-iT PicoGreen dsDNA assay (Thermo Fisher Scientific) and by low-pass sequencing with a MiSeq nano kit (Illumina). Paired-end 100 cycle sequencing was performed on the NovaSeq 6000 (Illumina) system.

TMT-based quantitative LC–MS proteomics and LC–MS data analysis

Two different clones of G401 cells expressing dTAG-DCAF5 were treated with DMSO or 50 nM of dTAG^{V-1} for 4 or 24 h in biological duplicate and cells were collected by centrifugation at 4 °C. The detailed protocol was performed as previously described⁵⁷ and is provided in the Supplementary Information.

Ubiquitylome analysis

TMT-based ubiquitinome analysis was performed on the basis of previously published methods^{58,59}. The detailed protocol for the following steps is available in the Supplementary Information: cell lysis and protein digestion, di-Gly peptide enrichment, TMT labelling and LC/LC–MS, and protein and di-Gly peptide identification and quantification using the JUMP software suite.

Protein expression and purification

For the DDB1-DDA1–DCAF5 complex, the following human gene combinations were used: DDB1ΔB (residues 396–705 replaced with a GNGNSG linker)⁶⁰, full-length DCAF5 (UniProt: Q96JK2) and full-length DDA1 (UniProt: Q9BW61). For the CRL4–DCAF5 complex, the human genes used were full-length *DDB1* (UniProt: Q16531), *DCAF5* (N-terminal domains 1–477, 1–601 or full length), full-length *DDA1*, *CUL4A* (residues 38–759) (UniProt: Q16531) and *Mus musculus Rbx1* (residues 12–108) (UniProt: P62878). All these genes were cloned into pAC-derived vectors⁶¹ (BD Biosciences PharMingen). Baculovirus for protein expression (Invitrogen) was generated by transfection into *Spodoptera frugiperda* (Sf9) cells at a density of 0.9×10^6 cells per ml grown in ESF 921 medium (Expression Systems), followed by three rounds of infection in Sf9 cells to increase the viral titre⁶⁰. Recombinant proteins were expressed in *Trichoplusia ni* High Five insect cells by infection with high-titre baculovirus. High Five cells grown in SF-900 II SFM medium (Gibco) at a density of 2.0×10^6 cells per ml were infected with baculovirus at 1.5% (v/v) for 40 h at 27 °C. For the cBAF complex (Flag-ARID1A, SMARCE1, SMARCD1, SMARCB1, ACTL6A, DPF2, SMARCC1, SMARCC2, ACTB and SMARCA4)⁶², the corresponding human genes were co-transfected into suspension Expi293F cells according to the manufacturer's recommendation (Thermo Fisher Scientific). Cells were cultured for 72 h at 37 °C under 8% CO₂ and collected by centrifugation.

For purification, cells were resuspended in lysis buffer containing 50 mM Tris-HCl pH 8.0, 200 mM NaCl, 0.25 mM TCEP (Tris(2-carboxyethyl)phosphine), 1 mM PMSF and 1 tablet per 500 ml protease inhibitor cocktail (Sigma-Aldrich), and lysed by sonification. After ultracentrifugation, the soluble fraction was passed over the Strep-Tactin XT Superflow (IBA) affinity resin, eluted with wash buffer (50 mM Tris-HCl pH 8.0, 200 mM NaCl, 1 mM TCEP) supplemented with 50 mM d-biotin (IBA). The affinity-purified DDB1(ΔB1)–DDA1–DCAF5 or CRL4–DCAF5(1–601) complex used for structure determination was next applied to an ion-exchange column (Poros 50HQ, Thermo Fisher Scientific) and eluted in 50 mM Tris-HCl pH 8.5, 2 mM TCEP by a linear salt gradient (from 50–800 mM NaCl). Peak fractions from ion-exchange chromatography were then subjected to size-exclusion chromatography on the Superdex 200 10/300 Increase column in 50 mM HEPES pH 7.4 or pH 8.0, 200 mM NaCl and 2 mM TCEP.

The purified protein complexes were concentrated using ultrafiltration (Millipore) and flash-frozen in liquid nitrogen and stored at –80 °C.

Grid preparation and data collection

A total of 4 µl DDB1(ΔB)–DDA1–DCAF5 (0.9 mg ml⁻¹) was applied to a glow-discharged (PELCO easiGlow, 20 mA, 60 s, 39 Pa) Quantifoil 1.2/1.3 300 grid in a Leica EM-GP operated at 90% relative humidity. After 10 s pre-blot time, the protein was blotted for 3 s (with 4 s post-blot time) and vitrified in liquid ethane after 4 s post-blot time. Data were recorded on the Thermo Fisher Talos Arctica system operated at 200 kV equipped with a Gatan K3 direct electron detector. SerialEM⁶³ was used to record 1,072 videos (50 frames, 4.5 exposure time) at a nominal magnification of $\times 36,000$, with a total accumulated dose of 53.35 e⁻ Å⁻², and defocus ranging from –1.5 µm to –2.5 µm.

Data processing and model building

All processing was performed in cryoSPARC (v.3.3.2 and v.4.12)⁶⁴. All resolutions are given based on the Fourier shell correlation (FSC) 0.143 threshold criterion^{65,66}. In total, 1,072 movies were corrected for beam-induced motion and the contrast transfer function (CTF) was estimated on-the-fly in cryoSPARC live. 2D classes from live processing were used to train TOPAZ⁶⁷ particle picker, and 1,404,938 particles were extracted at 1.5 Å px⁻¹ from 1,068 curated micrographs. The extracted particles were cleaned with one round of heterogeneous refinement using one good reference and five decoy references. In total, 547,943 cleaned particles were re-extracted at 1.1 Å px⁻¹, per-particle defocus was determined and CTF parameters (tilt, trefoil, spherical aberration, tetrafoil) were optimized. These particles then yielded a reconstruction at 2.8 Å after local refinement using a mask encompassing the entire molecule. After one round of local motion correction in cryoSPARC (v.4.1.2), a final reconstruction at 2.6 Å was obtained after local refinement. The map, automatically sharpened with a *B*-value of –96.8 Å², as well as a map post-processed using deepEMhancer⁶⁸, were used for model building in COOT (v.0.9.8)⁶⁹. Initial models for DDB1 and DDA1 (Protein Data Bank (PDB): 6QOR)⁵⁹ as well as a structure prediction for DCAF5 from RoseTTAFold⁷⁰ were rigid-body-fitted into the density in ChimeraX (v.1.4)⁷¹, relaxed into the density using ISOLDE (v.1.3)⁷² and then adjusted manually in COOT with help from Rosetta (v.3.12)⁷³. The input structures were refined in torsion and Cartesian space with penalties for deviation from ideal bond angles and bond lengths. To the standard full-atom score function, a fit-to-density score term was added to maximize real-space correlations between the model and map. Density correlations were determined with interpolation on a pre-computed per-atom score grid⁷⁴. The command line used was as follows: \$ROSETTA3_BIN/rosetta_scripts.linuxgccrelease -in::file::s -parser::protocol relax_density_cart.xml -beta-out:nstruct 400 -edenisty::mapreso 2.8 -edenisty::cryoem_scatterers -crystal_refine.

Relax_density_cart.xml is supplied in the GitHub repository. The final model was refined using phenix.real_space_refine^{75,76} (v.1.19.2-4158) and the model and maps were deposited in the PDB (PDB: 8TL6) and the Electron Microscopy Data Bank (EMDB: EMD-41363), respectively. Interface areas were calculated using PDBePisa⁷⁷, structural similarity searches were conducted using PDBeFold⁷⁸ and all figures with models and density were generated in ChimeraX. Conservation scores were determined using ConSurf⁷⁹. The local resolution range is given based on the 0–75% percentile in local resolution histograms⁸⁰. Directional resolution was calculated using 3DFSC⁸¹. Structural biology applications used in this project were compiled and configured by SBGrid⁸².

In vitro neddylation of CRL4–DCAF5

In vitro neddylation of CRL4–DCAF5 complexes was performed as previously described^{83,84}. In brief, 4 µM of purified CRL4–DCAF5 was mixed with 0.2 µM E1(NAE1/UBA3), 1.2 µM E2(UBE2M) and 15 µM Nedd8 in a reaction buffer containing 50 mM Tris pH 7.5, 100 mM NaCl, 2.5 mM

MgCl₂, 5 mM ATP and 0.5 mM DTT. The reaction was carried out at room temperature for 2 h and full neddylation was confirmed by SDS-PAGE analysis. The neddylated CRL4–DCAF5 complex was subsequently purified using size-exclusion chromatography.

In vitro ubiquitylation assay

In vitro ubiquitylation reactions were performed in a total volume of 15 µl with E1 (UBA1, R&D Systems) at 0.2 µM (R&D Systems), the variable E2 enzyme at 0.5 µM each (UBE2D1, UBE2D2, UBE2D4, UBE2N, UBE2L3, UBE2D3, UBE2E1, UBE2G1, UBE2H, UBE2E3, UBE2R1, UBE2M or UBE2C; R&D Systems), Mg-ATP (R&D Systems) at 10 mM and ubiquitin at 50 µM (R&D Systems), and buffered with 1× E3 ligase reaction buffer (R&D Systems). The reactions were pre-incubated for 30 min to allow charging of the E2 and then initiated by addition of neddylated 0.5 µM CRL4–DCAF5 complex (as described above) and 2 µM testing substrate (cBAF or SMARCC1). The reactions were incubated for 120 min at 37 °C and quenched by the addition of SDS sample buffer and analysed by 4–20% SDS-PAGE⁸⁴ or western blotting using anti-substrate antibodies.

DCAF5 quantitative IP–MS and data analysis

The detailed protocol is provided in the Supplementary Information.

Computational analysis

The detailed process for the following experiments is available in Supplementary Information: CRISPR–Cas9 dependency screen analysis, NGS data processing, ChIP–seq, CUT&RUN, motif enrichment analysis, RNA-seq and AlphaFold Predictions.

Quantification and statistical analysis

GraphPad PRISM 9 and R (v.3.6.1) software packages were used to perform statistical analyses. Statistical tests used are specified in the figure legends. To perform statistical tests between experimental groups for RNA-seq, ChIP-seq, and ATAC-seq, trimmed mean of *M*-value scale factors were estimated using edgeR and a limma-voom, empirical bayes moderation to establish significant differences. Significant differential binding of SWI/SNF members was defined as: FC > 2 ($\log_2[FC] > 1$) and FDR < 0.05 and FC < 0.5 ($\log_2[FC] < -1$) and FDR < 0.05. Significant differentially expressed genes were defined as $\log_2[FC] > 0$ and FDR < 0.05 and $\log_2[FC] < 0$ and FDR < 0.05. Significant changes in accessibility were defined as $\log_2[FC] > 1$ and FDR < 0.05 and $\log_2[FC] < -1$ and FDR < 0.05.

Material availability

Plasmids and cell lines generated in this study are available on request after completion of a material transfer agreement. Limited quantities of generated DCAF5 polyclonal antibody are available on request after completion of a material transfer agreement.

Reporting summary

Further information on research design is available in the Nature Portfolio Reporting Summary linked to this article.

Data availability

The ChIP-seq, ATAC-seq and RNA-seq data supporting the findings of this study have been deposited in the GEO database under accession number GSE215025. MS-based proteomics raw data files are provided in Supplementary Tables 1–3 and 6–8, and are available at PRIDE under the following dataset identifiers: PXD046276 (Supplementary Table 1), PXD046275 (Supplementary Tables 2 and 3), PXD046273 (Supplementary Table 6) and PXD04646 (Supplementary Tables 7 and 8). Coordinates for DDB1ΔB–DDA1–DCAF5 have been deposited at the PDB under accession number 8Tl6. The cryo-EM volume data are available at the Electron Microscopy Data Bank under accession number EMD-41363. Source data are provided with this paper.

Code availability

The code for analysing the data and the relax_density_cart.xml has been deposited at GitHub (<https://github.com/jamyers2358/SWISNF.DCAF5.Dependency>)⁸⁵.

52. Stewart, E. et al. Targeting the DNA repair pathway in Ewing sarcoma. *Cell Rep.* **9**, 829–841 (2014).
53. Zheng, M. et al. Caspase-6 promotes activation of the caspase-11-NLRP3 inflammasome during Gram-negative bacterial infections. *J. Biol. Chem.* **297**, 101379 (2021).
54. Sidoli, S. et al. One minute analysis of 200 histone posttranslational modifications by direct injection mass spectrometry. *Genome Res.* **29**, 978–987 (2019).
55. Drosos, Y. et al. NSD1 mediates antagonism between SWI/SNF and polycomb complexes and is required for transcriptional activation upon EZH2 inhibition. *Mol. Cell* **82**, 2472–2489 (2022).
56. Connally, J. P. & Pruitt-Miller, S. M. CRISPy: a versatile and high-throughput analysis program for CRISPR-based genome editing. *Sci. Rep.* **9**, 4194 (2019).
57. McAlister, G. C. et al. MultiNotch MS3 enables accurate, sensitive, and multiplexed detection of differential expression across cancer cell line proteomes. *Anal. Chem.* **86**, 7150–7158 (2014).
58. Rose, C. M. et al. Highly multiplexed quantitative mass spectrometry analysis of ubiquityomes. *Cell Syst.* **3**, 395–403 (2016).
59. Yu, K. et al. High-throughput profiling of proteome and posttranslational modifications by 16plex TMT labeling and mass spectrometry. *Methods Mol. Biol.* **2228**, 205–224 (2021).
60. Faust, T. B. et al. Structural complementarity facilitates E7820-mediated degradation of RBM39 by DCAF15. *Nat. Chem. Biol.* **16**, 7–14 (2020).
61. Abdulrahman, W. et al. A set of baculovirus transfer vectors for screening of affinity tags and parallel expression strategies. *Anal. Biochem.* **385**, 383–385 (2009).
62. He, S. et al. Structure of nucleosome-bound human BAF complex. *Science* **367**, 875–881 (2020).
63. Schor, M., Haberbosch, I., Hagen, W. J. H., Schwab, Y. & Mastronarde, D. N. Software tools for automated transmission electron microscopy. *Nat. Methods* **16**, 471–477 (2019).
64. Punjani, A., Rubinstein, J. L., Fleet, D. J. & Brubaker, M. A. cryoSPARC: algorithms for rapid unsupervised cryo-EM structure determination. *Nat. Methods* **14**, 290–296 (2017).
65. Scheres, S. H. & Chen, S. Prevention of overfitting in cryo-EM structure determination. *Nat. Methods* **9**, 853–854 (2012).
66. Rosenthal, P. B. & Henderson, R. Optimal determination of particle orientation, absolute hand, and contrast loss in single-particle electron cryomicroscopy. *J. Mol. Biol.* **333**, 721–745 (2003).
67. Bepler, T. et al. Positive-unlabeled convolutional neural networks for particle picking in cryo-electron micrographs. *Nat. Methods* **16**, 1153–1160 (2019).
68. Sanchez-Garcia, R. et al. DeepEMhancer: a deep learning solution for cryo-EM volume post-processing. *Commun. Biol.* **4**, 874 (2021).
69. Emsley, P., Lohkamp, B., Scott, W. G. & Cowtan, K. Features and development of Coot. *Acta Crystallogr. D* **66**, 486–501 (2010).
70. Baek, M. et al. Accurate prediction of protein structures and interactions using a three-track neural network. *Science* **373**, 871–876 (2021).
71. Goddard, T. D. et al. UCSF ChimeraX: meeting modern challenges in visualization and analysis. *Protein Sci.* **27**, 14–25 (2018).
72. Croll, T. I. ISOLDE: a physically realistic environment for model building into low-resolution electron-density maps. *Acta Crystallogr. D* **74**, 519–530 (2018).
73. Leman, J. K. et al. Macromolecular modeling and design in Rosetta: recent methods and frameworks. *Nat. Methods* **17**, 665–680 (2020).
74. Wang, R. Y. et al. Automated structure refinement of macromolecular assemblies from cryo-EM maps using Rosetta. *eLife* **5**, e17219 (2016).
75. Adams, P. D. et al. PHENIX: a comprehensive Python-based system for macromolecular structure solution. *Acta Crystallogr. D* **66**, 213–221 (2010).
76. Afonine, P. V. et al. Real-space refinement in PHENIX for cryo-EM and crystallography. *Acta Crystallogr. D* **74**, 531–544 (2018).
77. Krissinel, E. & Henrick, K. Inference of macromolecular assemblies from crystalline state. *J. Mol. Biol.* **372**, 774–797 (2007).
78. Krissinel, E. & Henrick, K. Secondary-structure matching (SSM), a new tool for fast protein structure alignment in three dimensions. *Acta Crystallogr. D* **60**, 2256–2268 (2004).
79. Armon, A., Graur, D. & Ben-Tal, N. ConSurf: an algorithmic tool for the identification of functional regions in proteins by surface mapping of phylogenetic information. *J. Mol. Biol.* **307**, 447–463 (2001).
80. Cardone, G., Heymann, J. B. & Steven, A. C. One number does not fit all: mapping local variations in resolution in cryo-EM reconstructions. *J. Struct. Biol.* **184**, 226–236 (2013).
81. Tan, Y. Z. et al. Addressing preferred specimen orientation in single-particle cryo-EM through tilting. *Nat. Methods* **14**, 793–796 (2017).
82. Morin, A. et al. Collaboration gets the most out of software. *eLife* **2**, e01456 (2013).
83. Duda, D. M. et al. Structural insights into NEDD8 activation of cullin-RING ligases: conformational control of conjugation. *Cell* **134**, 995–1006 (2008).
84. Fischer, E. S. et al. Structure of the DDB1–CRBN E3 ubiquitin ligase in complex with thalidomide. *Nature* **512**, 49–53 (2014).
85. Radko-Juettner, S. et al. Targeting DCAF5 suppresses SMARCB1-mutant cancer by stabilizing SWI/SNF. GitHub <https://github.com/jamyers2358/SWISNF.DCAF5.Dependency> (2024).

Acknowledgements This work was supported by grants from the National Cancer Institute (NCI) (R01 CA113794, R01 CA273455 and R01 CA172152) to C.W.M.R.; CURE AT/RT Now to C.W.M.R.; the Garrett B. Smith Foundation to C.W.M.R.; and the St Jude Children's Research Hospital Collaborative Research Consortium on Chromatin Regulation in Pediatric Cancer to C.W.M.R. S.R.-J. is supported by the St Jude Graduate School of Biomedical Sciences and the Ruth L. Kirschstein National Research Service Award (F31 CA261150); B.N. by the National

Article

Cancer Institute (NCI) (K22 CA258805); E.S.F. by grants from the National Cancer Institute (NCI) (R01 CA262188); J.P. by the National Institute on Aging (RF1AG068581). We thank members of the Roberts laboratory and S. Thiom for discussions; G. Riddihough for assistance with editing this manuscript; C. Guy for assistance with microscopy; N. Thomä for the recombinant CBAF complex plasmids; the staff at Harvard Center for Cryo-Electron Microscopy for their support during grid screening and data collection; the members of the SBGrid Consortium for assistance with software and high-performance computing; and the members of the following St Jude core facilities: the Peptide Synthesis Core, the Protein Production Facility for Cas9, the Animal Resources Center for animal care, the Transgenic Core, the Flow Cytometry and Cell Sorting Shared Resource for FACS sorting, the Hartwell Center for Biotechnology for sequencing and peptide synthesis, the Center for In Vivo Imaging and Therapeutics for in vivo imaging and the Vector Development and Production Core for virus preparation. The St Jude Core facilities are supported by National Cancer Institute Cancer Center Support Grant (NCI CCSG 2 P30 CA021765) and by American Lebanese Syrian Associated Charities (ALSAC) of St Jude Children's Research Hospital. The Center for Applied Bioinformatics is supported by the National Cancer Institute, Cancer Center Support Grant P30 CA21765 and ALSAC. The content is solely the responsibility of the authors and does not necessarily represent the official views of the National Institutes of Health.

Author contributions S.R.-J. conceived the study, designed and performed the experiments, analysed the data, interpreted the results and wrote the manuscript. H.Y. performed DCAF5 structural studies, in vitro ubiquitylation assays, analysed results, provided intellectual input and wrote the manuscript. J.A.M. performed computational analysis, interpreted the results, assisted with manuscript writing and wrote computational methods. R.D.C. performed cellular experiments, assisted with mouse experiments, analysed the data and interpreted the results. A.N.R. performed cellular experiments, analysed the data and assisted with mouse experiments. P.M. assisted with growth assays, mouse experiments and colony management. Z.Z. assisted with ChIP-seq experiments and optimization. B.S.H. generated the CRISPR-edited pools and analysed the CRISPR fitness assay results. K.A.D. performed TMT profiling and AP-MS processing, analysed the data and interpreted the results. M.H. assisted with DCAF5 structural experiments and data processing. W.R. performed computational analysis, interpreted the results and wrote computational methods. Z.W. and M.G.M. assisted with ubiquitinome analysis and data processing. S.S.R.B. assisted with AlphaFold predictions and Rosetta refinement for the DCAF5 structure. A.M.S. performed LC-MS processing and analysed the data. N.M. performed TMT-profiling. S.A.B. assisted in DCAF5 antibody design and validation. R.J.M. performed SMARCB1 CUT&RUN and created SMARCB1 re-expression cell

lines. J.F.P. provided intellectual input. E.A.S. assisted with in vivo study design and data analysis. S.M.P.-M. designed the CRISPR fitness assay and guides. B.N. and N.S.G. synthesized and provided the dTAG^{Y-1} in vitro and in vivo molecules and assisted in dTAG-DCAF5 design. J.P. assisted with ubiquitinome analysis, data processing and data interpretation. E.S.F. supervised the DCAF5 structural studies and in vitro ubiquitylation assays, analysed the TMT-profiling data, interpreted the results, provided intellectual input and wrote the manuscript. C.W.M.R. conceived the study, designed the experiments, interpreted the results, wrote the manuscript, and supervised and funded the study. All of the authors read, reviewed and approved the final manuscript.

Competing interests C.W.M.R. is a scientific advisory board member of Exo Therapeutics, unrelated to this Article. E.S.F. is a founder, scientific advisory board member and equity holder of Civetta Therapeutics, Neomorph (also board member) and Proximity Therapeutics, scientific advisory board member and equity holder in Avilar Therapeutics and Photys Therapeutics, equity holder in Lighthorse Therapeutics and is a consultant to Novartis, Sanofi, EcoRI capital, Ajax Therapeutics and Deerfield. The E.S.F. laboratory receives or has received research funding from Astellas, Novartis, Ajax, Voronoi, Interline and Deerfield on topics unrelated to this manuscript. B.N. is listed as an inventor on patent applications related to the dTAG system (WO/2017/024318, WO/2017/024319, WO/2018/148440 and WO/2018/148443). B.N. and N.S.G. are inventors on a patent related to the dTAG system and molecules described in this Article (WO/2020/146250). N.S.G. is a founder, science advisory board member and equity holder in Syros, C4 Therapeutics, Allorion, Lighthorse, Voronoi, Inception, Matchpoint, CobroVentures, GSK (scientific advisory board member), Larkspur (board member), Shenandoah (board member) and Soltego (board member). The N.S.G. laboratory receives or has received research funding from Novartis, Takeda, Astellas, Taiho, Jansen, Kinogen, Arbella, Deerfield and Sanofi on topics unrelated to this Article. K.A.D. is a consultant to Kronos Bio and Neomorph. The other authors declare no competing interests.

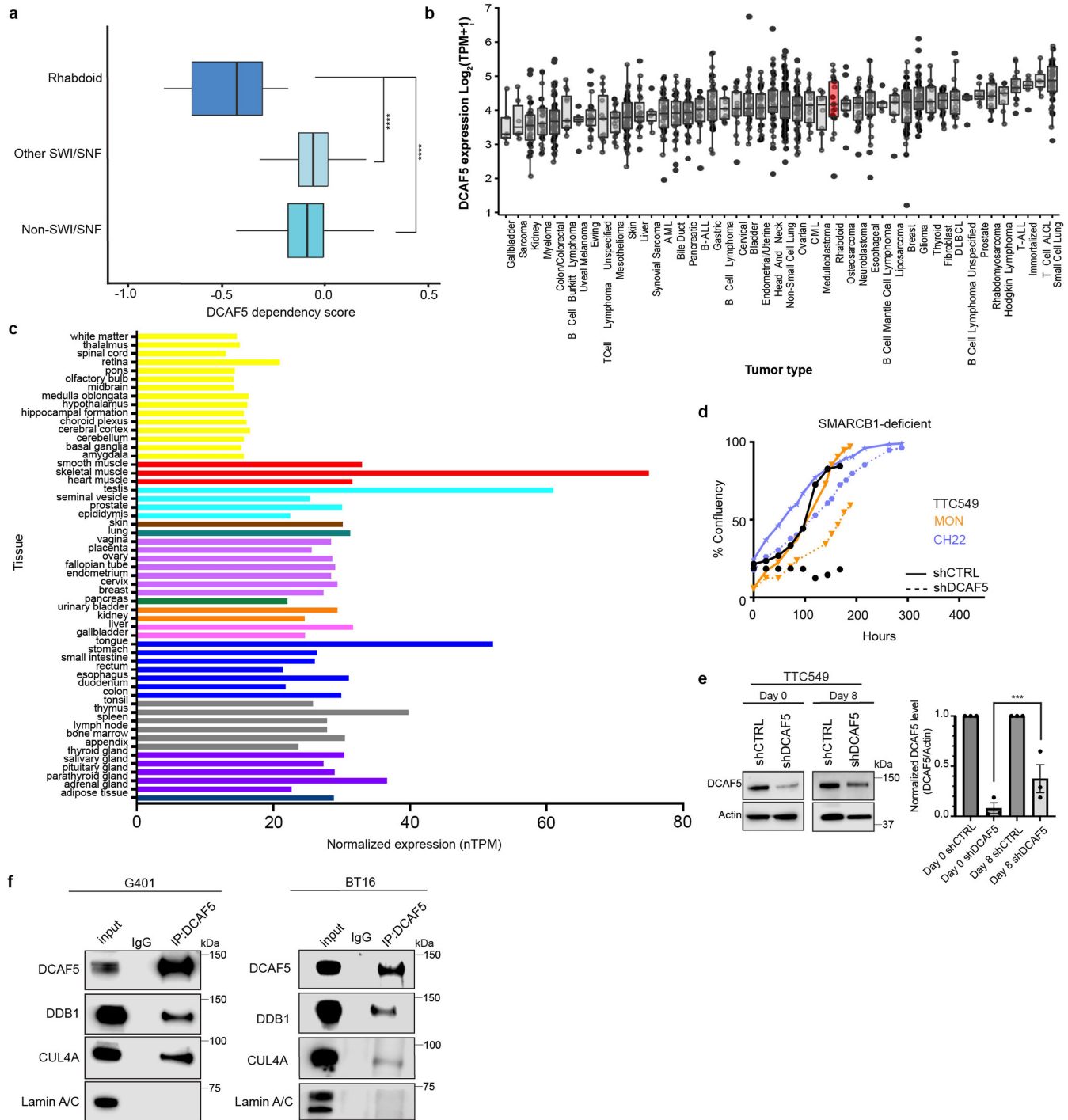
Additional information

Supplementary information The online version contains supplementary material available at <https://doi.org/10.1038/s41586-024-07250-1>.

Correspondence and requests for materials should be addressed to Eric S. Fischer or Charles W. M. Roberts.

Peer review information *Nature* thanks Tom Owen-Hughes and the other, anonymous, reviewer(s) for their contribution to the peer review of this work.

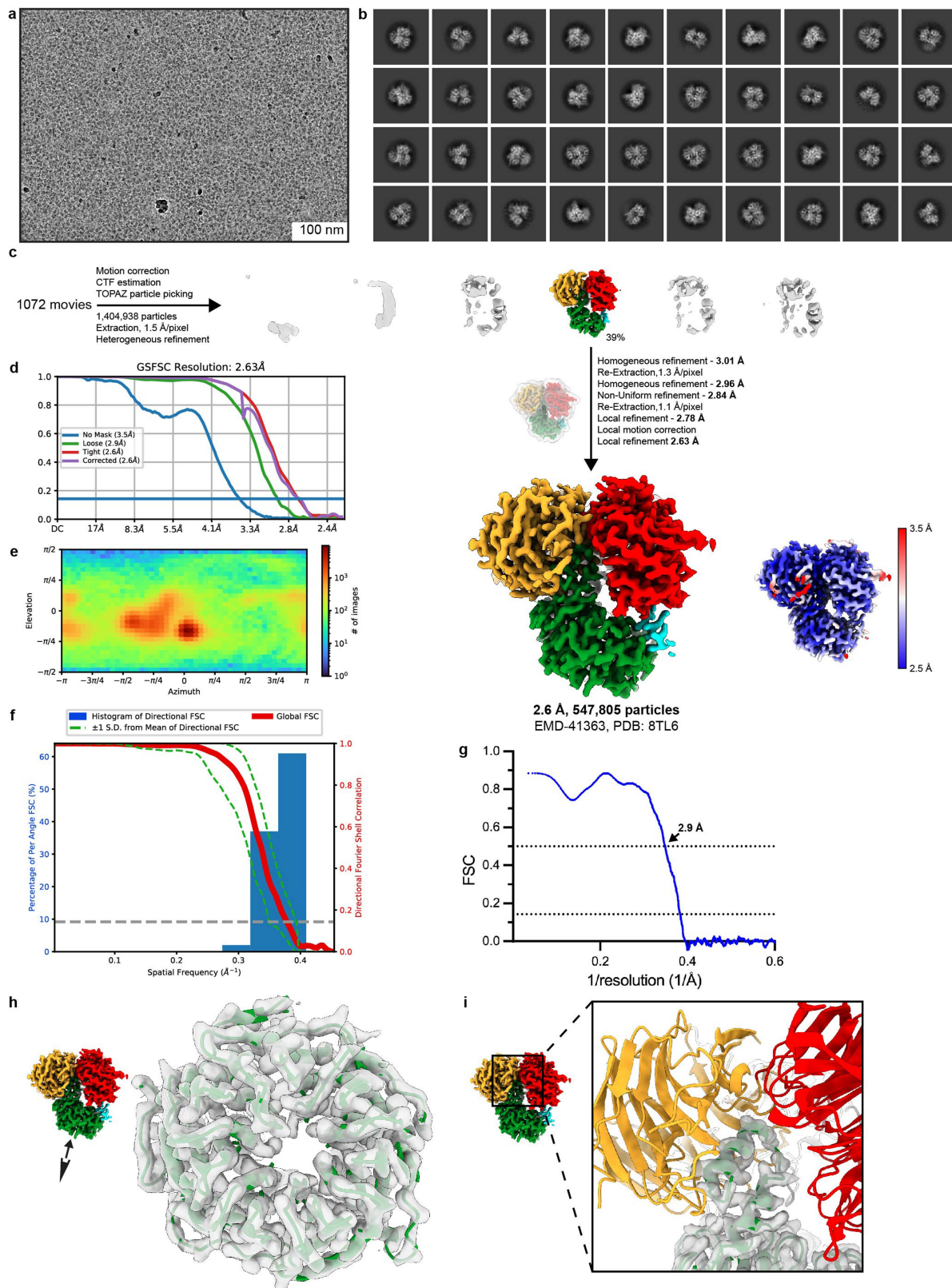
Reprints and permissions information is available at <http://www.nature.com/reprints>.



Extended Data Fig. 1 | DCAF5 dependence is specific to SMARCB1-mutant cancers independent of mRNA expression and tissue type. **a**, Two-class comparison of $n = 14$ biologically independent Rhabdoid Tumour cell lines compared to other SWI/SNF mutant cancer cell lines ($n = 190$) or other non-SWI/SNF mutant cancer cell lines ($n = 607$) ($****P = 1.22 \times 10^{-16}$ and 7.16×10^{-21} respectively; two-tailed Student's *t* test, release CERES 21Q1). The box plot indicates the median (centre line), the third and first quartiles (box limits) and $1.5 \times$ interquartile range (IQR) above and below the box (whiskers). **b**, Box plot showing DCAF5 RNA expression across $n = 1332$ biologically independent cancer cell lines from different tumour types in the Cancer Cell Line Encyclopedia (CCLE) database. RT cell lines are shaded in red. The box plot indicates the median (centre line), the third and first quartiles (box limits) and $1.5 \times$ interquartile range (IQR) above and below the box (whiskers). **c**, Bar plot demonstrating normalized expression (nTPM) levels of DCAF5 for $n = 55$ tissue

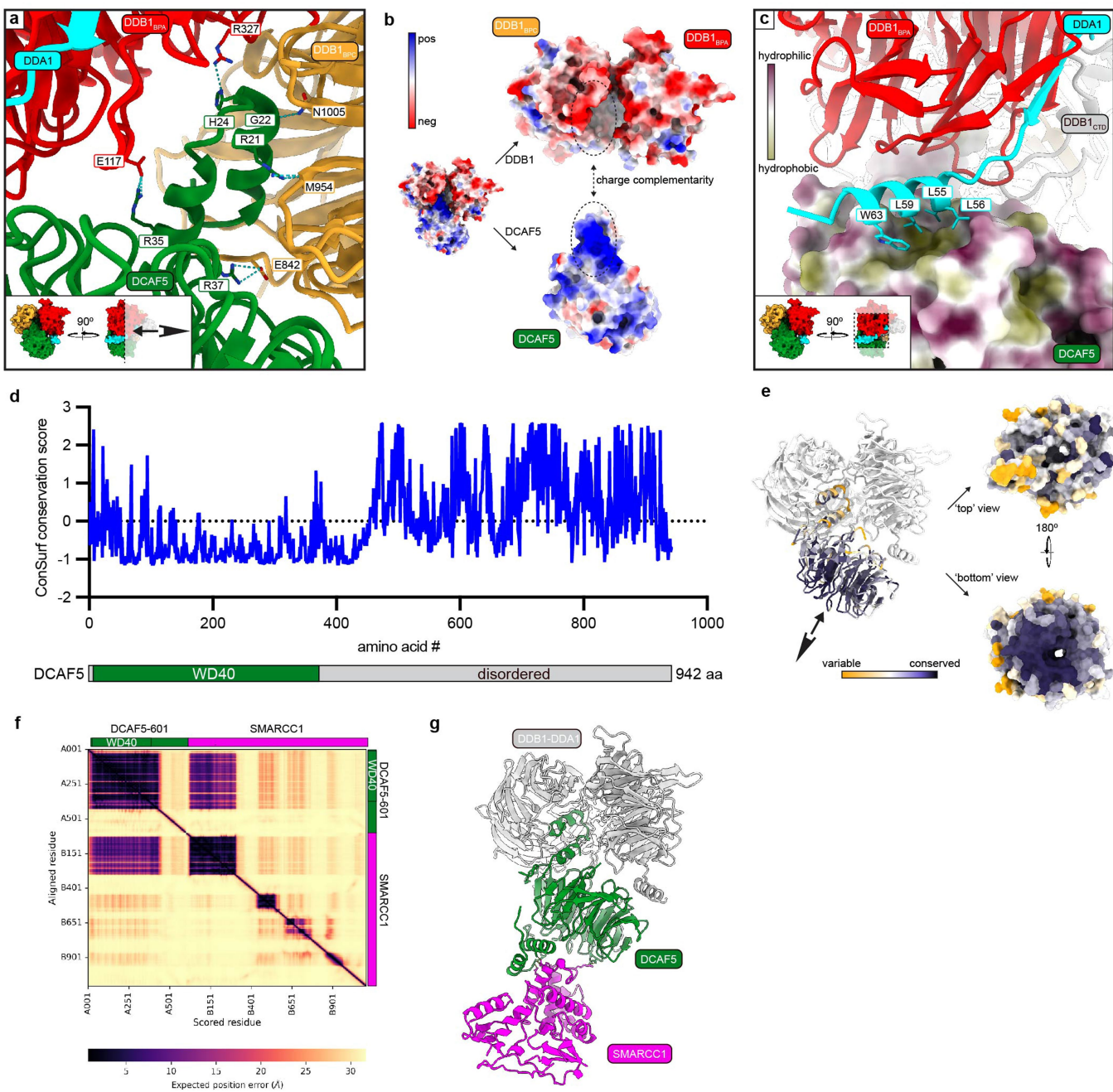
types, created by combining the HPA and GTEx transcriptomics datasets using the Human Protein Atlas internal normalization pipeline. Colour-coding is based on tissue groups. **d**, Effects on proliferation upon DCAF5 shRNA knockdown in SMARCB1-mutant cell lines. Solid lines (shCTRL) and dotted lines (shDCAF5). Graphs show mean values from $n = 8$ technical replicates per cell line condition from one independent biological experiment. **e**, Western blot analysis of TTC549 RT cell line at Day 0 and Day 8 of IncuCyte proliferation assay. Band intensities were quantified by the Licor Image Studio Lite software and then the normalized DCAF5 level was calculated relative to Actin and normalized to shControl signal \pm s.e.m ($n = 3$ independent biological replicates). $***P = 0.001$; Two-Way ANOVA. **f**, DCAF5 immunoprecipitation in G401 and BT16 RT cell line demonstrates interaction of DCAF5 with E3 Ub Ligase machinery. Input is 1% of the protein used for the IP ($n = 2$ independent biological replicates).

Article



Extended Data Fig. 2 | Cryo-EM processing workflow for the DDB1 Δ B-DDA1-DCAF5 structure. **a**, Raw micrograph (low pass-filtered to 10 Å, scale bar indicated). **b**, Representative 2D classes. **c**, Overview of processing workflow from raw micrograph. All processing steps were conducted in cryoSPARC. Particles belonging to coloured volumes were taken for the final map (EMD-41363). The final map is contoured at 0.134, and local resolution

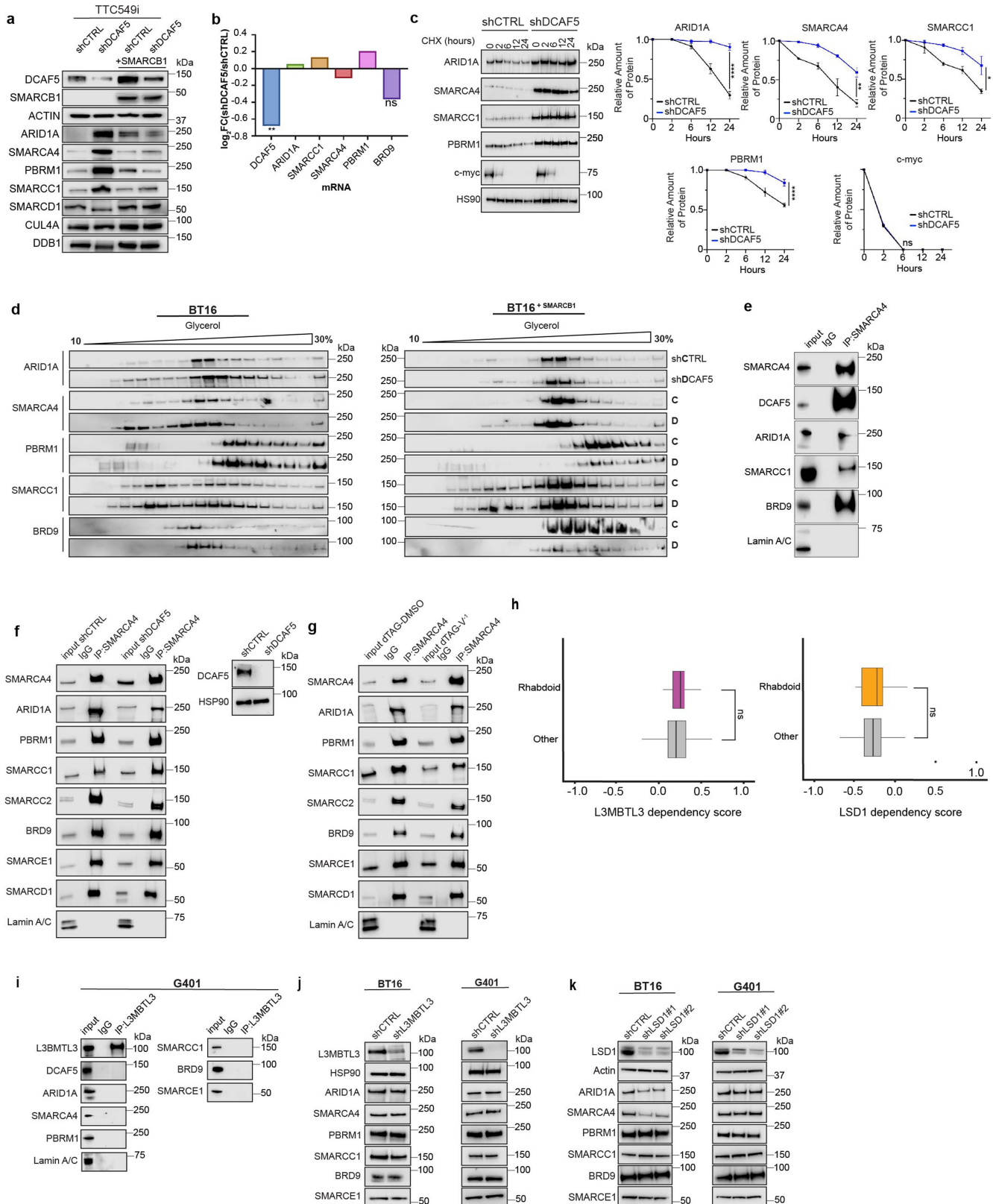
mapped onto the final reconstruction is shown. **d**, FSC plot for the deposited map (EMD-41363). **e**, Viewing distribution plot. **f**, Directional resolution histogram and directional FSC plot. **g**, Model-to-map FSC for the deposited structure (PDB: 8TL6), value given for FSC (model)=0.5. **h**, Density example for the DCAF5 WD40 domain. **i**, Density for the DCAF5 WD40 domain in the DDB1 Δ B binding site.



Extended Data Fig. 3 | Details of DDB1ΔB-DDA1-DCAF5 structure, evolutionary analysis and AlphaFold prediction. **a**, Detailed view of DCAF5 and DDB1ΔB interaction shown in cartoon representation. The N-terminal α -helix of DCAF5 tightly inserts into the pocket of DDB1. **b**, Charge complementarity between DCAF5 and DDB1 at the interface. **c**, The N terminus of DDA1 inserts into DDB1, while the C terminus of DDA1 binds DCAF5 tightly with a hydrophobic interaction. DCAF5 surface is shown with hydrophobic and hydrophilic colour coding. **d**, Plot of the ConSurf conservation score versus the amino acid residue of full-length DCAF5 with domain annotations. **e**, ConSurf

conservation scores are mapped onto DCAF5 with orange-white-purple colour scale in increasing conservation order. Top view and bottom view of the WD40 domain are shown. **f**, AlphaFold predictions for the DCAF5 aa 1-601 and SMARCC1 interaction. In the domain bar, DCAF5 is represented in green, with the WD40 domain specifically highlighted. SMARCC1 is depicted in magenta. **g**, The AlphaFold predicted binding mode of DCAF5 and SMARCC1 is shown. DCAF5 is represented in green, SMARCC1 is depicted in magenta, and DDB1-DDA1 is represented in grey.

Article

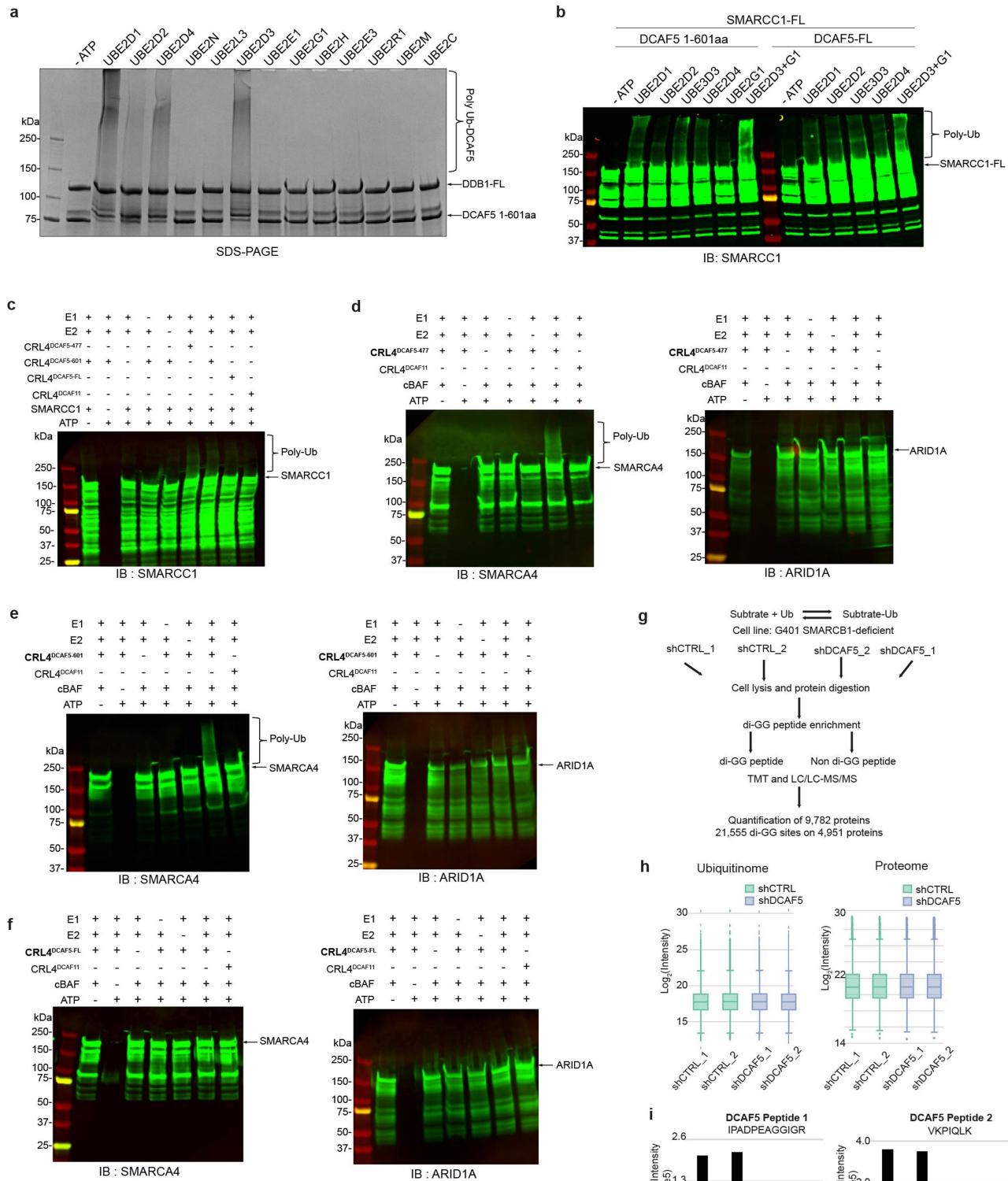


Extended Data Fig. 4 | See next page for caption.

Extended Data Fig. 4 | DCAF5 loss upregulates protein levels of SWI/SNF members and alters SWI/SNF complex integrity. **a**, Western blot analysis of SWI/SNF subunits in TTC549 SMARCB1-inducible RT cells treated with shCTRL or shDCAF5 after 72 h selection in the presence or absence of SMARCB1. **b**, RNA-Seq analysis in G401RT cells treated with shCTRL or shDCAF5 after 72 h selection evaluating log₂ fold change of mRNA for SWI/SNF in shDCAF5 versus shCTRL. ns = not significant; **log₂FC = -0.68, FDR = 0.02. Significance was determined by two-sided Empirical Bayes test for differential expression with FDR adjusted p-values. **c**, Left: Cycloheximide Chase (0–24 h with 50 µg/mL cycloheximide) in G401shCTRL or shDCAF5 evaluating SWI/SNF subunit levels and control protein c-myc. Right: Graphical representation of the cycloheximide experimental data for the mean relative protein amount ± s.e.m of ARID1A (****P = < 0.0001), SMARCA4 (**P = < 0.0022), SMARCC1 (*P = < 0.0180), PBRM1 (****P = < 0.0001) and c-myc (P = ns: not significant); Two-Way ANOVA. **d**, Glycerol gradient (10–30% glycerol) analysis of SMARCB1-deficient BT16 RT cells treated with either shCTRL or shDCAF5 after 72 h selection (top panel). SMARCB1 has been re-expressed in the cells in the bottom panel. **e**, SMARCA4 co-immunoprecipitation in G401shCTRL and shDCAF5 conditions demonstrates that the SWI/SNF complex is maintained in the absence of DCAF5. Lamin A/C

is a negative control. Input is 1% of the protein used for the IP. **f**, SMARCA4 co-immunoprecipitation in G401-dTAG-DCAF5 cells treated with DMSO and v-1 demonstrates retained SWI/SNF complex interactions in the absence of DCAF5. Lamin A/C is a negative control. Input is 1% of the protein used for the IP. **g**, SMARCA4 co-immunoprecipitation in G401RT cells demonstrates interaction with DCAF5 and SWI/SNF subunits. Lamin A/C is a negative control. Input is 1% of the protein used for the IP. **h**, Two-class comparison of n = 14 biologically independent Rhabdoid Tumour cell lines compared to n = 789 biologically independent other cancer cell lines in DepMap analysing L3MBTL3 and LSD1 dependency (P = 0.907 and 0.701 respectively and is non-significant (ns); two-tailed Student's t test, release CERES 21Q1). The box plots indicate the median (centre line), the third and first quartiles (box limits) and 1.5 × interquartile range (IQR) above and below the box (whiskers). **i**, L3MBTL3 co-immunoprecipitation in G401RT cells detects no interaction with DCAF5 or SWI/SNF subunits. **j**, Western blot analysis of SWI/SNF subunits in BT16 and G401RT cells treated with shCTRL or shL3MBTL3 after 72 h selection. **k**, Western blot analysis of SWI/SNF subunits in BT16 and G401RT cells treated with shCTRL or shLSD1 after 72 h selection. Data are representative of three (**c**) or two (**d,e,f,g,i,j** and **k**) independent biological experiments.

Article

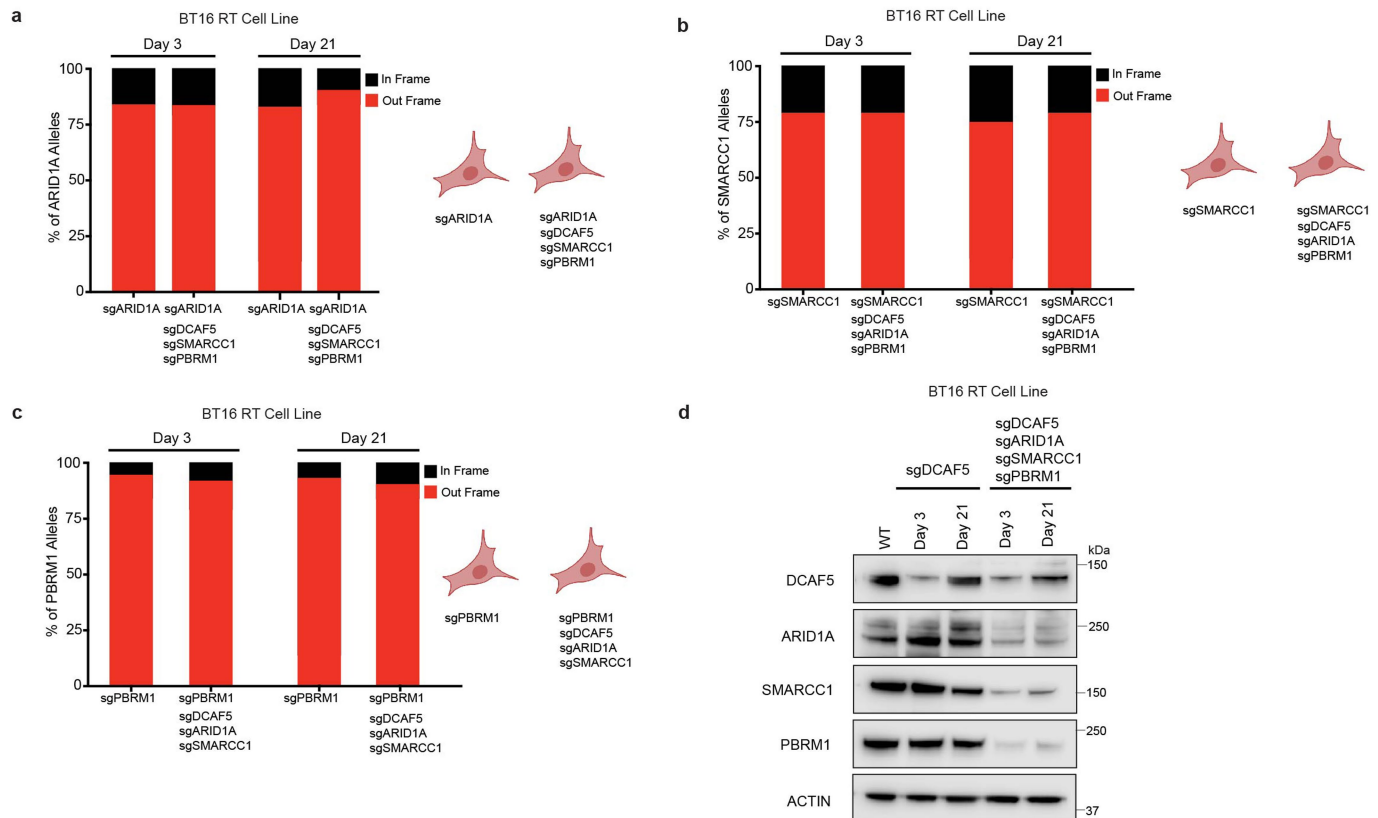


Extended Data Fig. 5 | See next page for caption.

Extended Data Fig. 5 | In vitro and in vivo analyses of CRL4-DCAF5 and SWI/SNF substrates. **a**, In vitro ubiquitylation assay screening of 13 E2-conjugating enzymes for CUL4-DDB1-RBX1-DCAF5 (CRL4^{DCAF5}) ligase autoubiquitylation ($n = 2$). FL= full-length. **b**, In vitro ubiquitylation assay screening E2-conjugating enzymes for ubiquitylation of full-length (FL) SMARCC1 by FL-DCAF5 and DCAF5_aa1-601). The combination of UBE2D3 + UBE2G1 has previously been identified as a canonical E2 pair for CRL4 ligases. **c**, In vitro ubiquitylation assay of SMARCC1 with 3 different CUL4^{DCAF5} constructs: DCAF5_aa1-477 (which contains only the putatively active WD40 domain), DCAF5_aa1-601 (which contains an extended region), and FL-DCAF5, alongside the CRL4^{DCAF11} complex (another ring E3 ligase) as a negative control and the whole recombinant SWI/SNF complex for ubiquitylation. The UBE2D3/UBE2G1 combination is chosen as the E2 pair for this assay and the following ubiquitylation assays. **d**, In vitro ubiquitylation assay of SMARCA4 (left) and ARID1A (right) in recombinant cBAF complex with CUL4^{DCAF5_aa1-477} (which contains only the putatively active WD40 domain) complex. The experiment

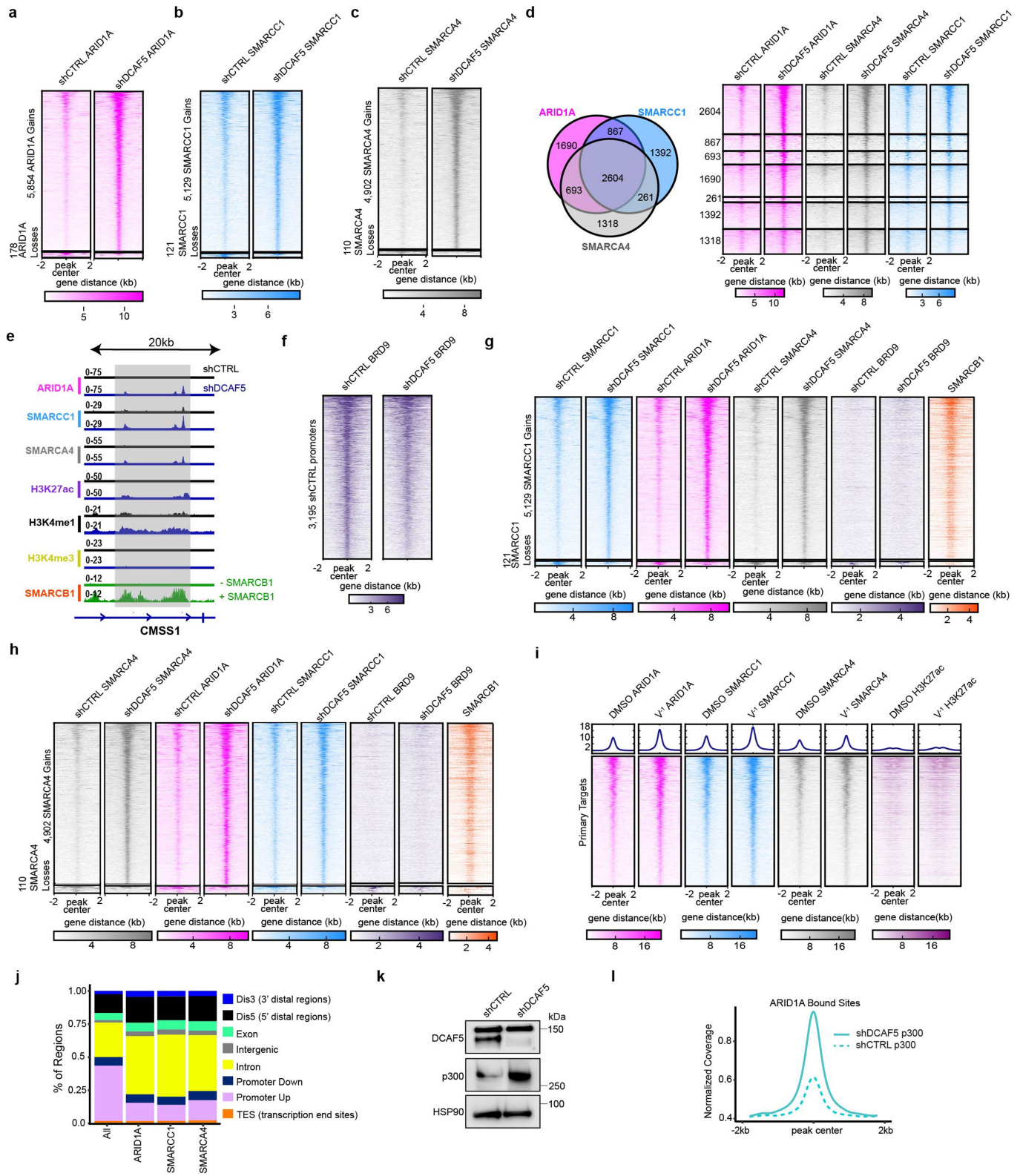
has been performed once. **e**, In vitro ubiquitylation assay of SMARCA4 (left) and ARID1A (right) in recombinant cBAF complex with CUL4^{DCAF5_aa1-601} (which contains an extended region) complex. **f**, In vitro ubiquitylation assay of SMARCA4 (left) and ARID1A (right) in recombinant cBAF complex with full-length CUL4^{DCAF5_FL} complex. The experiment has been performed once. **g**, Workflow of ubiquitylome analysis in G401 shCTRL and shDCAF5 RT cells. **h**, Comparison of global MS intensities in whole proteome and ubiquitylome ($n = 2$ biological replicates). Similar \log_2 values of intensities indicate minimal sample loading bias in both datasets. The boxplots of ubiquitinome and proteome were from $n = 44,752$ Peptide Spectrum Matches (PSMs) and $n = 390,548$ PSMs respectively. The box plots indicate the median (centre line), the third and first quartiles (box limits) and $1.5 \times$ interquartile range (IQR) above and below the box (whiskers). **i**, MS intensities of two DCAF5 peptides indicate significant downregulation of DCAF5 protein in G401shDCAF5 samples. Data are representative of two (**a,c**, and **e**) or three (**b**) independent biological experiments.

Article



Extended Data Fig. 6 | CRISPR-mediated knockout of DCAF5 SWI/SNF substrates rescues the lethal phenotype. **a**, Indel toxicity assay evaluating selection against *ARID1A* out-of-frame alleles (containing *ARID1A* knockout) either in BT16 SMARCB1-deficient RT cells or in BT16 SMARCB1-deficient RT cells in which residual SWI/SNF subunits *ARID1A*, *PBRM1*, *SMARCC1* and *DCAF5* have been inactivated by CRISPR guides. CRISPR knockout of *ARID1A* is tolerated in both instances. **b**, Indel toxicity assay evaluating selection against *SMARCC1* out-of-frame alleles (containing *SMARCC1* knockout) either in BT16 SMARCB1-deficient RT cells or in BT16 SMARCB1-deficient RT cells in which residual SWI/SNF subunits *SMARCC1*, *PBRM1*, *ARID1A* and *DCAF5* have been inactivated by CRISPR guides. CRISPR knockout of *SMARCC1* is tolerated in both instances. **c**, Indel toxicity assay evaluating selection against *PBRM1* out-of-frame alleles (containing *PBRM1* knockout) either in BT16 SMARCB1-deficient RT cells or in BT16 SMARCB1-deficient RT cells in which residual SWI/SNF subunits *PBRM1*, *SMARCC1*, *ARID1A* and *DCAF5* have been inactivated by CRISPR guides. CRISPR knockout of *PBRM1* is tolerated in both instances.

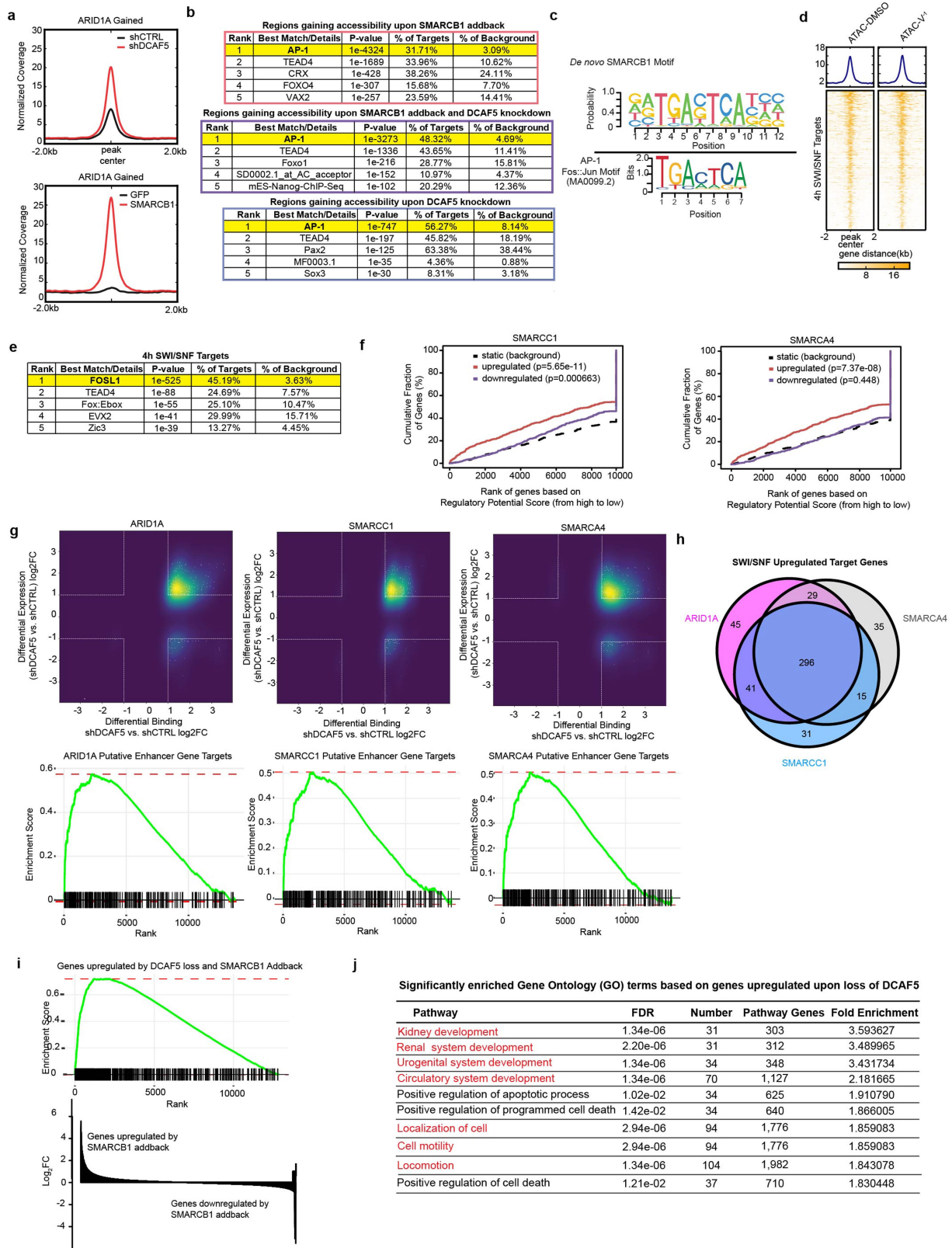
both instances. **c**, Indel toxicity assay evaluating selection against *PBRM1* out-of-frame alleles (containing *PBRM1* knockout) either in BT16 SMARCB1-deficient RT cells or in BT16 SMARCB1-deficient RT cells in which residual SWI/SNF subunits *PBRM1*, *SMARCC1*, *ARID1A* and *DCAF5* have been inactivated by CRISPR guides. CRISPR knockout of *PBRM1* is tolerated in both instances. **d**, Western blot analysis in BT16-SMARCB1-deficient RT cells at Day 3 versus Day 21 in which residual SWI/SNF subunits *ARID1A*, *PBRM1*, *SMARCC1* and *DCAF5* have been inactivated by CRISPR guides. WT are wildtype cells. Data are representative of three independent biological experiments. Diagrams in **a**, **b**, and **c** were created using BioRender (<https://biorender.com/>).



Extended Data Fig. 7 | See next page for caption.

Article

Extended Data Fig. 7 | SWI/SNF binding increases upon DCAF5 loss at enhancer regions. **a**, Peak centred heatmaps \pm 2 kb of averaged normalized coverage for significant, differentially bound regions defined as $FC > 2$ and $FDR < 0.05$ for ARID1A ($n = 3$ independent biological replicates) upon DCAF5 loss in G401RT cells. **b**, Peak centred heatmaps \pm 2 kb of averaged normalized coverage for significant, differentially bound regions defined as $FC > 2$ and $FDR < 0.05$ for SMARCC1 ($n = 3$ independent biological replicates) upon DCAF5 loss in G401RT cells. **c**, Peak centred heatmaps \pm 2 kb of averaged normalized coverage for significant, differentially bound regions defined as $FC > 2$ and $FDR < 0.05$ for SMARCA4 ($n = 2$ independent biological replicates) upon DCAF5 loss in G401RT cells. **d**, Venn Diagram of gained regions ($FC > 2$ and $FDR < 0.05$) for ARID1A, SMARCC1, and SMARCA4. Peak centred heatmap \pm 2 kb of averaged normalized coverage at each set of regions defined within the Venn Diagram. **e**, Sample locus depicting gains in averaged normalized coverage of SWI/SNF subunits and various histone marks in shDCAF5 treated G401RT cells compared to control. **f**, Peak centred heatmaps \pm 2 kb of averaged normalized coverage at 3,195 promoters for BRD9 in shCTRL ($n = 2$ independent biological replicates) and shDCAF5 ($n = 2$ independent biological replicates). **g**, Peak centred heatmaps \pm 2 kb of averaged normalized coverage for SWI/SNF subunits at significant, differentially bound regions defined as $FC > 2$ and $FDR < 0.05$ for SMARCC1 in G401RT cells. **h**, Peak centred heatmaps \pm 2 kb of averaged normalized coverage for SWI/SNF subunits at significant, differentially bound regions defined as $FC > 2$ and $FDR < 0.05$ for SMARCA4 in G401RT cells. **i**, Peak centred heatmaps \pm 2 kb of averaged normalized coverage for SWI/SNF subunits ($n = 1$ independent biological replicate per mark) and H3K27ac ($n = 2$ independent biological replicates) 4 h after DCAF5 degradation with $v\cdot 1$ ($FC > 0$) at a previously defined subset of differentially bound regions. **j**, Genomic feature distribution of the entire genome (All) and ARID1A, SMARCC1, and SMARCA4 gained regions upon DCAF5 loss ($FC > 2$ and $FDR < 0.05$). **k**, Western blot analysis of p300 levels in G401RT cells treated with shCTRL or shDCAF5 ($n = 2$ independent biological replicates). **l**, Peak centred metaplot of normalized, average coverage for p300 ($n = 3$ independent biological replicates) centred (\pm 2 kb) on regions significantly gaining ARID1A upon loss of DCAF5 in G401 RT cells. Gains of p300 coincide with gains of H3K27ac upon loss of DCAF5.

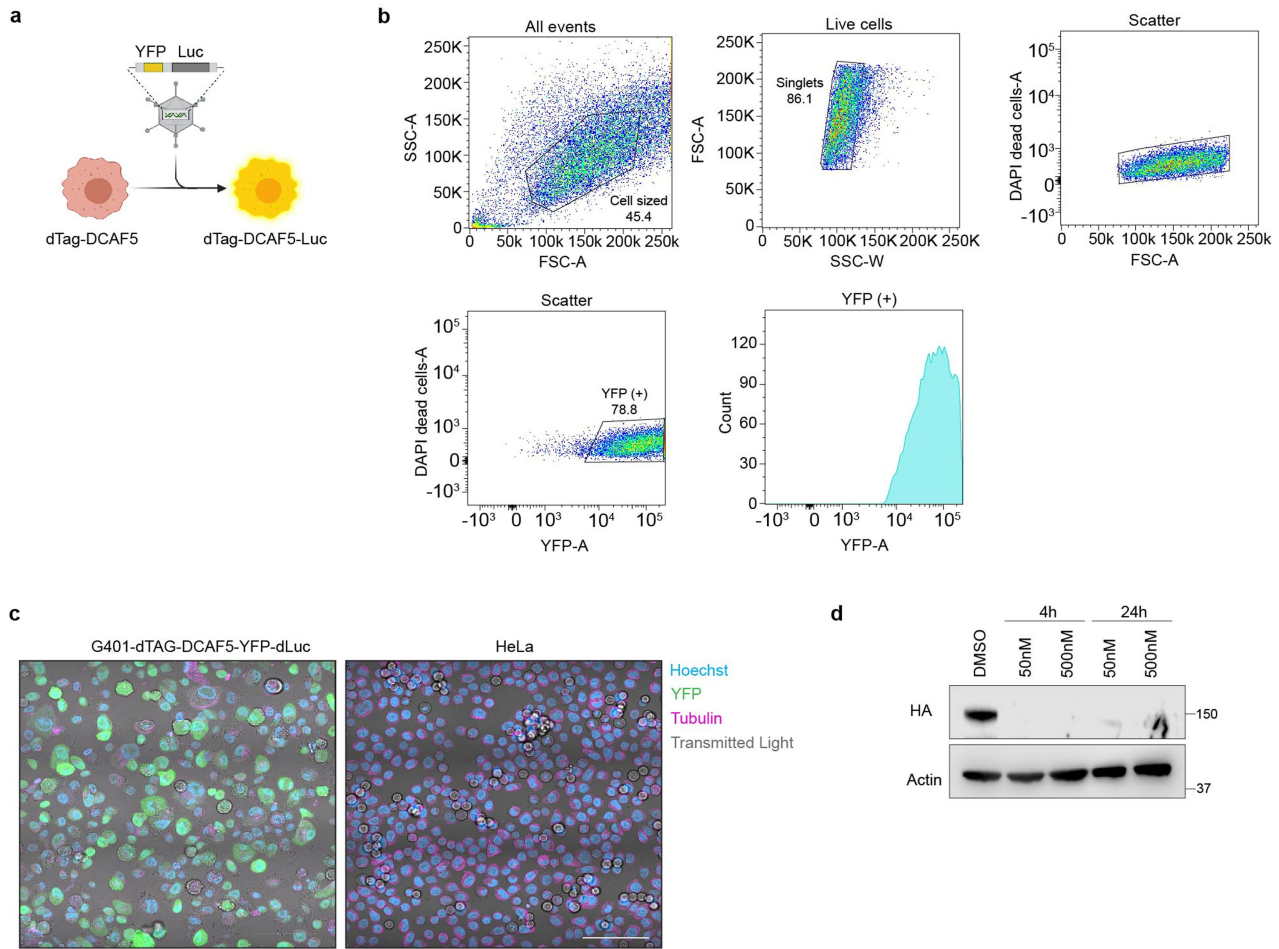


Extended Data Fig. 8 | See next page for caption.

Article

Extended Data Fig. 8 | Following DCAF5 loss, increased SWI/SNF binding results in transcriptional activation. **a**, Peak centred metaplots of ARID1A gained regions ($FC > 2$, $FDR < 0.05$) ± 2 kb of averaged normalized nucleosome free coverage from ATAC-Seq for G401 shCTRL ($n = 3$ independent biological replicates) and shDCAF5 ($n = 3$ independent biological replicates) treated cells (left) compared to G401 \sim SMARCB1 inducible cells (right) ($n = 3$ independent biological replicates). **b**, Motif enrichment analysis at regions gaining accessibility at SWI/SNF bound regions in SMARCB1 re-expressed cells, within the sites gained in both SMARCB1 addback and DCAF5 loss conditions and in shDCAF5 cells. P-values were calculated with a cumulative binomial distribution (one-sided) with Benjamini multiple test correction. **c**, Alignment of the position weight matrix (PWM) for the most significantly enriched de novo motif with the known AP-1 PWM (MA0099.2). **d**, Peak centred, ± 2 kb heatmaps at previously defined 4 h SWI/SNF gained regions ($FC > 0$) of averaged normalized nucleosome free coverage for G401-dTAG-DCAF5 DMSO treated ($n = 3$ independent biological replicates) and γ -1 ($n = 3$ independent biological replicates) treated cells. **e**, Motif enrichment analysis at regions gaining SWI/SNF binding 4 h after DCAF5 degradation in G401-dTAG-DCAF5 cells. P-values were calculated with a cumulative binomial distribution (one-sided) with Benjamini multiple test correction. **f**, Relationship between transcriptional regulation (RNA-Seq) and gained binding of SMARCC1 and SMARCA4 upon loss of DCAF5 (ChIP-Seq) in G401 RT cells by Binding and Expression Target Analysis (BETA). Red and blue lines represent activated and repressed genes

respectively and the dashed line represents an unchanging gene set. P-values calculated with one-tailed Kolmogorov-Smirnov test and compare the activated and repressed genes to the unchanging set. Predicted SMARCC1 and SMARCA4 target genes are upregulated upon DCAF5 loss. **g, Top:** Relationship between transcriptional changes (RNA-Seq) shDCAF5 vs. shCTRL log₂FC y-axis and differential binding of shDCAF5 vs. shCTRL ARID1A, SMARCC1, and SMARCA4 (ChIP-Seq) log₂FC x-axis. **Bottom:** GSEA results comparing gene sets of the top 500 ARID1A, SMARCC1, and SMARCA4 putative enhancer gene targets bound in shDCAF5 treated G401 cells, defined based on log₂FC, $-\log_{10}(p\text{-value})$, and $\log_{10}(\text{Mean Enrichment} + 1)$, to transcriptional changes upon loss of DCAF5 in G401 RT cells, p-value: 0.002, 0.002, 0.002 and normalized enrichment score (NES): 2.37, 2.08, 2.08, respectively. Nominal P-value estimated using an empirical gene set permutation test. **h**, Venn diagram of predicted ARID1A, SMARCC1, and SMARCA4 upregulated target genes (predicted by BETA). **i**, GSEA results comparing a gene set of upregulated genes upon loss of DCAF5 in G401 RT cells ($\log_2 FC > 0$ and adjusted p-value < 0.05) to the expression changes upon SMARCB1 re-expression in G401 RT cells (GSE71506) p-value = 0.001 and NES = 2.32. Nominal P-value estimated using an empirical gene set permutation test. **j**, Significantly enriched Gene Ontology (GO) terms ranked on Fold Enrichment (binomial over/under representation test with Bonferroni correction), based on genes significantly upregulated upon loss of DCAF5 in G401 RT cells ($\log_2 FC > 0$ and adjusted p-value < 0.05). Pathways labelled in red are also upregulated upon SMARCB1 re-expression.



Extended Data Fig. 9 | Generation and validation of G401-dTAG-DCAF5-YFP-dLuc cells. **a**, Schematic of YFP-luciferase integration into G401-dTAG-DCAF5 cells. **b**, Flow cytometry plots and gating strategy for sorting G401-dTAG-DCAF5-YFP-dLuc cells that are YFP+. **c**, Immunofluorescence confirmation of YFP expression in G401-dTAG-DCAF5-YFP-dLuc cells compared to HeLa YFP negative control cells. Scale bar 100 μ m. The experiment has been performed once. **d**, Western blot analysis confirming

DCAF5 degradation of G401-dTAG-DCAF5-YFP-dLuc cells after treatment with 50 nM or 500 nM of dTAG^{V-1} at 4 h and 24 h. The experiment has been performed once. **e**, Weight comparisons from 8-week-old *Dcaf5* female mice ($n=5$ mice per genotype). WT (wildtype), Het. (heterozygous) and KO (knockout) $P=ns$ (non-significant); Two-way ANOVA. The diagram in **a** was created using BioRender (<https://biorender.com/>).

Article

Extended Data Table 1 | Cryo-EM data collection, refinement and validation statistics

DCAF5-DDB1ΔB-DDA1 (EMDB-41363) (PDB 8TL6)	
Data collection and processing	
Magnification	36,000x
Voltage (kV)	200
Electron exposure (e-/Å ²)	53.35
Defocus range (μm)	-1.5 - -2.5
Pixel size (Å)	1.1
Symmetry imposed	C1
Initial particle images (no.)	1,404,938
Final particle images (no.)	547,943
Map resolution (Å)	2.6
FSC threshold	0.143
Map resolution range (Å)	2.5-5.8
Refinement	
Initial model used (PDB code)	6Q0R, roseTTAfold, de novo
Model resolution (Å)	2.9
FSC threshold	0.5
Model resolution range (Å)	2.5-5.8
Map sharpening <i>B</i> factor (Å ²)	-96,8
Model composition	
Non-hydrogen atoms	9,320
Protein residues	1,177
Ligands	-
<i>B</i> factors (Å ²)	
Protein	41.71
Ligand	-
R.m.s. deviations	
Bond lengths (Å)	0.002
Bond angles (°)	0.516
Validation	
MolProbity score	1.39
Clashscore	4.53
Poor rotamers (%)	0
Ramachandran plot	
Favored (%)	97.06
Allowed (%)	2.94
Disallowed (%)	0.00

Reporting Summary

Nature Portfolio wishes to improve the reproducibility of the work that we publish. This form provides structure for consistency and transparency in reporting. For further information on Nature Portfolio policies, see our [Editorial Policies](#) and the [Editorial Policy Checklist](#).

Statistics

For all statistical analyses, confirm that the following items are present in the figure legend, table legend, main text, or Methods section.

n/a Confirmed

- The exact sample size (n) for each experimental group/condition, given as a discrete number and unit of measurement
- A statement on whether measurements were taken from distinct samples or whether the same sample was measured repeatedly
- The statistical test(s) used AND whether they are one- or two-sided
Only common tests should be described solely by name; describe more complex techniques in the Methods section.
- A description of all covariates tested
- A description of any assumptions or corrections, such as tests of normality and adjustment for multiple comparisons
- A full description of the statistical parameters including central tendency (e.g. means) or other basic estimates (e.g. regression coefficient) AND variation (e.g. standard deviation) or associated estimates of uncertainty (e.g. confidence intervals)
- For null hypothesis testing, the test statistic (e.g. F , t , r) with confidence intervals, effect sizes, degrees of freedom and P value noted
Give P values as exact values whenever suitable.
- For Bayesian analysis, information on the choice of priors and Markov chain Monte Carlo settings
- For hierarchical and complex designs, identification of the appropriate level for tests and full reporting of outcomes
- Estimates of effect sizes (e.g. Cohen's d , Pearson's r), indicating how they were calculated

Our web collection on [statistics for biologists](#) contains articles on many of the points above.

Software and code

Policy information about [availability of computer code](#)

Data collection

Immunoblot chemiluminescent images were acquired using Li-COR ImageStudio software (v5.5.4). Cell confluency values were obtained using the Incucyte instrument and software, GUI 2022A Rev1. Sequencing reads were obtained using the Illumina Novaseq 6000. Bioluminescent images were taken using the IVIS 200 imaging system. The Living Image 4.3 software (Caliper Life Sciences) was used to generate a standard region of interest (ROI). Single cell clones were obtained using the Aria cell sorter (BD Biosciences) and analyzed with FlowJo 5.4+ version 10. TMT data were collected using an Orbitrap Fusion Lumos mass spectrometer (Thermo Fisher Scientific, San Jose, CA, USA) coupled with a Proxeon EASY-nLC 1200 LC pump (Thermo Fisher Scientific, San Jose, CA, USA). Peptides were separated on a 50 cm 75 μ m inner diameter EasySpray ES903 microcapillary column (Thermo Fisher Scientific).

NGS processing tools:

Traim-galore (v0.4.4), bwa aln/samse/sampe (v0.7.12-r103995), samtools (v1.2), STAR (2.7.1a), bamsormadup biobambam (v2.0.87), SPP(v1.11), bedtools (v2.24.0), UCSC tools (v4), MACS2 (v2.1.1.20160309), deeptools (v2.5.3), BETA (v1.0.7), VennDiagram (v1.6.20), R (v3.6.1), pheatmap (v1.0.12), edgeR (v3.28.0) ggplot(2.3.3.2) IGV (v2.11.3), samtools (v1.2), ShinyGO (v0.76), fgsea(v1.19.4), limma(3.42.2), pybedtools(v0.8.1), homer (v4.9.1)

Cry-EM structure: cryoSPARCv3.3.2 and v4.12, COOTv0.9.8, RoseTTAFold, ChimeraXv1.4, ISOLDeV1.3, Rosetta v3.12, phenix.real_space_refine32,33 (v.1.19.2-4158), validation(Interface areas by PDBePisa, structural similarity by PDBeFold), Conservation scores by ConSurf.

AlphaFold Predictions : AlphaFold v2.3 (DeepMind)

Proteomics processing tools:Proteome Discoverer 2.5, R (v4.2.2), Rstudio (v2022.07.1), limma (v3.54.2), ggplot2 (v3.4.3), dplyr (v1.1.3), gplots (3.1.3), tidyverse (v1.3.0)

Data analysis

The code for analyzing the data and the relax_density_cart.xml has been deposited in GitHub (<https://github.com/jamyers2358/>)

Data analysis

SWISNF.DCAF5.Dependency).

TMT results were analyzed using Proteome Discoverer 2.5 (Thermo Fisher Scientific) was used for .RAW file processing and controlling peptide and protein level false discovery rates, assembling proteins from peptides, and protein quantification from peptides. The MS/MS spectra were searched against a Swissprot human database (January 2021) containing both the forward and reverse sequences.

ChIP-Seq Analysis

Raw reads in fastq format were processed with Trim-Galore tool (v0.4.4, Krueger F. (2012), Available online: https://www.bioinformatics.babraham.ac.uk/projects/trim_galore/), to remove potential adapters and quality trim 3' end of reads with cutadapt program10, followed by FastQC analysis (<http://www.bioinformatics.babraham.ac.uk/projects/fastqc/>). A quality score cutoff of Q20 was used. ChIP-Seq reads were mapped to human-drosophila reference hybrid genome (merged hg19/GRCh37.p13 and dm6 genomes) with bwa aln, followed by bwa samse (v0.7.12-r103911) with -K flag set to 10000000, and the output was converted to BAM format with samtools (v1.2.12). Cross-Correlation analysis was conducted with SPP (v1.1116). Uniquely mapped reads were then extracted with samtools12, extended with bedtools (v2.24.0,17) using the fragment size value previously estimated with Cross-Correlation analysis, and then converted to bigwig track files by UCSC tools (v418). For the visualization purposes only, the mapped reads' densities were converted to BigWig format and normalized to 15 million non-duplicated mapped reads and the average signal between biological replicates was calculated to be displayed in the main figure panels.

Peaks were called using MACS219 program with –nomodel -q 0.05 flags (high confidence peaks). Separately, narrow peaks were also called with more relaxed criteria, setting the -q flag to 0.5 (low confidence peaks). Following the previously described approach20, the reproducible peaks of biological replicates were identified as those which either in both replicates had overlapping high confidence peaks or those, which in one replicate had a high confidence peak, which was supported by a high- or low-confidence peak in all other replicates. In each case the coordinates of the final reproducible peak are based on the union of the coordinates of high confidence peaks. Finally, reproducible peaks were annotated using reference gene annotation from Gencode v1913, if they overlap the gene promoters, which was done with bedtools (v2.24.017), one region could be assigned to multiple genes. These are considered putative promoter-related regions. The promoter regions were defined as TSS ± 2 kbp. Next, regions not assigned to any gene promoter, were assigned to gene as putative enhancer-related regions, if their distance to gene's TSS was within a threshold of ± 50 kbp, excluding the promoter region. One region could be assigned to multiple genes. In parallel, reproducible peaks were also annotated with genomic contexts one-by-one, with the following prioritization order:

1. Promoter.Up - Region up to 2 kbp upstream from the TSS.
2. Promoter.Down - Region down to 2 kbp downstream from the TSS.
3. Exon - all exons, from any isoform.
4. Intron - all introns, from any isoform.
5. TES (transcription end sites) - region spanning TES (a.k.a TTS, transcription termination site) +/- 2 kbp.
6. Dis5 (5' distal regions) - region up to 50 kbp upstream from TSS, excluding promoter region.
7. Dis3 (3' distal regions) - region down to 50 kbp downstream from TES.
8. Intergenic - all remaining regions, excluding alternative chromosomes that lack any known reference annotation.

The number of fragments for each reference peak were calculated with intersect command from pybedtools and used as input for downstream differential testing. All heat maps and metaplots of normalized, averaged coverage were generated using deeptools (v2.5.322) using the reference-point mode with computeMatrix (-a, -b 2000), plotHeatmap and plotProfile (-ooutFileNameData). Additionally, the metaplots were generated in R using ggplot2 with a gaussian smoother using the deeptools plotProfile output, normalizing the signal coverage to the H3K27ac shDCAF5 maximum signal. The integrative genome viewer (IGV v. 2.11.323) was used to visualize changes in SWI/SNF binding at specific loci.

Regions significantly gaining (FDR < 0.05 and FC >2) binding of SWI/SNF were annotated with the average q-value of individual replicate peaks using bedtools map (v2.25.017) to represent the binding strength. Binding scores for each SWI/SNF mark were integrated with the log2FC and FDR of expression changes shDCAF5 vs. shCTRL using (BETA v.1.0.724) to predict active/repressed gene targets. A Venn diagram (VennDiagram v1.6.20, <https://CRAN.R-project.org/package=VennDiagram>) was generated to visualize and define a common set of gene targets for all three SWI/SNF members. Hierarchically clustered and z-score centered heat map was generated using pheatmap (<https://CRAN.R-project.org/package=pheatmap>). Gene ontology enrichment analysis was performed (ShinyGO v0.76) on the 296 conserved predicted SWI/SNF up-regulated target genes.

Pre-ranked GSEA was performed using fgsea (v1.19.425) in R. The log2FC ranked gene lists were either transcriptional changes upon 48hr SMARCB1 add back or loss of DCAF5. Several custom gene sets were defined (1) genes up-regulated upon loss of DCAF5 log2FC > 0 and adjusted p-value < 0.05 or (2) top 500 genes associated with putative enhancers (within 2-50kb) ranked based on log2FC, -log10(p-value), and log10(Mean enrichment +1) for ARID1A (3) top 500 genes associated with putative enhancers (within 2-50kb) ranked based on log2FC, -log10(p-value), and log10(Mean enrichment +1) for SMARCC1, (4) top 500 genes associated with putative enhancers (within 2-50kb) ranked based on log2FC, -log10(p-value), and log10(Mean enrichment +1) for SMARCA4.

For manuscripts utilizing custom algorithms or software that are central to the research but not yet described in published literature, software must be made available to editors and reviewers. We strongly encourage code deposition in a community repository (e.g. GitHub). See the Nature Portfolio [guidelines for submitting code & software](#) for further information.

Data

Policy information about [availability of data](#)

All manuscripts must include a [data availability statement](#). This statement should provide the following information, where applicable:

- Accession codes, unique identifiers, or web links for publicly available datasets
- A description of any restrictions on data availability
- For clinical datasets or third party data, please ensure that the statement adheres to our [policy](#)

The ChIP-seq, ATAC-seq and RNA-seq data that support the findings of this study have been deposited in the GEO database under the accession number GSE215025. Mass spectrometry-based proteomics raw data files are provided in Supplementary Table 1, 5-6 &9-11, and are available at PRIDE with the following dataset identifiers : Supplementary Table 1: PXD046276, Supplementary Table 5-6: PXD046275, Supplementary Table 9: PXD046273 and Supplementary Table 10-11: PXD04646. Coordinates for DDB1ΔB-DDA1-DCAF5 have been deposited in the PDB under accession numbers 8TL6. The cryo-EM volume data are available at the Electron Microscopy Data Bank under accession numbers EMD-41363.

Research involving human participants, their data, or biological material

Policy information about studies with [human participants or human data](#). See also policy information about [sex, gender \(identity/presentation\), and sexual orientation](#) and [race, ethnicity and racism](#).

Reporting on sex and gender

Not applicable to this study.

Reporting on race, ethnicity, or other socially relevant groupings

Not applicable to this study.

Population characteristics

Not applicable to this study.

Recruitment

Not applicable to this study.

Ethics oversight

Not applicable to this study.

Note that full information on the approval of the study protocol must also be provided in the manuscript.

Field-specific reporting

Please select the one below that is the best fit for your research. If you are not sure, read the appropriate sections before making your selection.

Life sciences Behavioural & social sciences Ecological, evolutionary & environmental sciences

For a reference copy of the document with all sections, see nature.com/documents/nr-reporting-summary-flat.pdf

Life sciences study design

All studies must disclose on these points even when the disclosure is negative.

Sample size

For ChIP-Seq, RNA-Seq and ATAC-seq analysis we targeted minimum of n=3 biological replicates consistent with the ENCODE guidelines. For all in vivo experiments, power analysis was carried out to determine cohort sizes for each treatment arm. Animal studies were also carried out respecting the limited use of animals in line with the 3R system: Replacement, Reduction, Refinement. Immunoprecipitation mass spectrometry and global proteomics experiments were performed in biological duplicates or biological triplicates. Through in-house empirical training datasets we have determined that duplicates combined with the limma package's empirical Bayesian approach to shrink the variance towards a common mean allows for sufficient variance estimations in screening for putative substrates. For TMT profiling and in vivo ubiquitylome studies no statistical methods were used to predetermine sample sizes; however, the sample sizes were comparable to those in prior studies (<https://pubmed.ncbi.nlm.nih.gov/34739326/>). Statistical methods were utilized to calculate p values. Upon applying the cutoffs for p values and fold changes, we identified protein changes of statistical significance as anticipated.

Data exclusions

One replicate of H3K27ac shCTRL and BRG1 shCTRL were discarded due to low enrichment quality that was determined by Cross Correlation analysis manifesting in a low QTAG score.

Replication

All attempts at replication were successful, except for one replicate of H3K27ac shCTRL and BRG1 shCTRL were discarded due to low enrichment quality that was determined by Cross Correlation analysis manifesting in a low QTAG score. The number of replicates for each experiment is stated in figure legends.

Randomization

Randomization was carried out for in vivo xenograft studies, where animals were randomized and enrolled into treatment arms using a blocked randomization list (<https://www.sealedenvelope.com/simple-randomiser/v1/lists>) when animals met enrollment criteria. For all other experiments we did not carry out randomization as this is either irrelevant or not applicable to this study.

Blinding

Blinding was not done since this study requires the investigator to study differences in cell lines.

Reporting for specific materials, systems and methods

We require information from authors about some types of materials, experimental systems and methods used in many studies. Here, indicate whether each material, system or method listed is relevant to your study. If you are not sure if a list item applies to your research, read the appropriate section before selecting a response.

Materials & experimental systems

n/a	Involved in the study
<input type="checkbox"/>	<input checked="" type="checkbox"/> Antibodies
<input type="checkbox"/>	<input checked="" type="checkbox"/> Eukaryotic cell lines
<input checked="" type="checkbox"/>	<input type="checkbox"/> Palaeontology and archaeology
<input type="checkbox"/>	<input checked="" type="checkbox"/> Animals and other organisms
<input checked="" type="checkbox"/>	<input type="checkbox"/> Clinical data
<input checked="" type="checkbox"/>	<input type="checkbox"/> Dual use research of concern
<input checked="" type="checkbox"/>	<input type="checkbox"/> Plants

Methods

n/a	Involved in the study
<input type="checkbox"/>	<input checked="" type="checkbox"/> ChIP-seq
<input type="checkbox"/>	<input checked="" type="checkbox"/> Flow cytometry
<input checked="" type="checkbox"/>	<input type="checkbox"/> MRI-based neuroimaging

Antibodies

Antibodies used

SMARCA4/BRG1 (Rabbit Monoclonal, Cell Signaling Technology, 49360, D1Q7F, Lot #3, 1:1000 WB dilution)
<https://www.cellsignal.com/products/primary-antibodies/brg1-d1q7f-rabbit-mab/49360>

SMARCA4/BRG1 (Rabbit Monoclonal, Abcam, ab110641 EPNCIR111A, Lot #1000647-8, 5ug for IP, 5ug for ChIP)
<https://www.abcam.com/products/primary-antibodies/brg1-antibody-epncir111a-ab110641.html>

SMARCC1/BAF155 (Rabbit Monoclonal, Cell Signaling Technology, 11956, D7F8S, Lot #5, 1:1000 WB dilution)
<https://www.cellsignal.com/products/primary-antibodies/smarcc1-baf155-d7f8s-rabbit-mab/11956>

SMARCC1/BAF155 (Rabbit Polyclonal, Thermo Fisher Scientific, PA5-30174, Lot #TG2606435C, 5ug for ChIP)
<https://www.thermofisher.com/antibody/product/SMARTCC1-Antibody-Polyclonal/PA5-30174>

SMARCC2/BAF170 (Rabbit Polyclonal, Cell Signaling Technology, 8829, Lot #1, 1:1000 WB dilution)
<https://www.cellsignal.com/products/primary-antibodies/smarcc2-baf170-antibody/8829>

ARID1A/BAF250a (Rabbit Monoclonal, Cell Signaling Technology, 12354, D2A8U, Lot #4, 1:1000 WB dilution)
<https://www.cellsignal.com/products/primary-antibodies/arid1a-baf250a-d2a8u-rabbit-mab/12354>

ARID1A/BAF250a (Rabbit Polyclonal, Sigma-Aldrich, HPA005456, Lot #114190 and 000041044, 5ug for ChIP)
<https://www.sigmal Aldrich.com/US/en/product/sigma/hpa005456>

ARID1B (Rabbit Monoclonal, Cell Signaling Technology, 92964, E9J4T, Lot #1, 1:1000 WB dilution)
<https://www.cellsignal.com/products/primary-antibodies/arid1b-baf250b-e9j4t-rabbit-mab/92964>

ARID2/BAF200 (Rabbit Monoclonal, Cell Signaling Technology, 82342, D8D8U, Lot #1, 1:1000 WB dilution)
<https://www.cellsignal.com/products/primary-antibodies/arid2-d8d8u-rabbit-mab/82342>

PBRM1/BAF180 (Rabbit Polyclonal, Bethyl, A301-591A, Lot #5, 1:1000 WB dilution)
<https://www.thermofisher.com/antibody/product/PBRM1-Antibody-Polyclonal/A301-591A>

SMARCE1/BAF57 (Rabbit Monoclonal, Cell Signaling Technology, 33360, E6H5J, Lot #1, 1:1000 WB dilution)
<https://www.cellsignal.com/products/primary-antibodies/smarce1-baf57-e6h5j-rabbit-mab/33360>

SMARCD1/BAF60a (Rabbit Polyclonal, Bethyl, A301-595A, Lot #2, 1:1000 WB dilution)
<https://www.fortislife.com/cms/files/A301-594A-T-1.pdf>

SMARCB1/SNF5/BAF47 (Rabbit Monoclonal, Cell Signaling Technology, 91735, D8M1X, Lot #2, 1:1000 WB dilution, 1 ul Cut & Run)
<https://www.cellsignal.com/products/primary-antibodies/smarcb1-baf47-d8m1x-rabbit-mab/91735>

BRD9 (Rabbit Monoclonal, Cell Signaling Technology, 58906, E9R2I, Lot #1, 1:1000 WB dilution)
<https://www.cellsignal.com/products/primary-antibodies/brd9-e9r2i-rabbit-mab/58906>

GLTSCR1 (Mouse Monoclonal, Santa Cruz Biotechnology, sc-515086, H-10, Lot #31220, WB: 1:250)
<https://www.scbt.com/p/gltsr1-antibody-h-10>

HSP90 (Rabbit Monoclonal, Cell Signaling Technology, 4877, C45G5, Lot #7, 1:1000 WB dilution)
<https://www.cellsignal.com/products/primary-antibodies/hsp90-c45g5-rabbit-mab/4877>

β-Actin (Mouse Monoclonal, Sigma-Aldrich, A5441, AC-15, Batch #000182451, 1:1000 WB dilution)
<https://www.sigmal Aldrich.com/US/en/product/sigma/a5441>

Lamin A/C (Mouse Monoclonal, Cell Signaling Technology, 4777, 4C11, Lot #5, 1:1000 WB dilution)
<https://www.cellsignal.com/products/primary-antibodies/lamin-a-c-4c11-mouse-mab/4777>

Normal IgG (Rabbit, Cell Signaling Technology, 2729, Lot #9, 5ug IP dilution)
<https://www.cellsignal.com/products/primary-antibodies/normal-rabbit-igg/2729>

Histone H3 acetyl (Lys27) (Rabbit Polyclonal, Abcam, ab4729, Lot #GR3252404-1, 5ug for ChIP)
<https://www.abcam.com/products/primary-antibodies/histone-h3-acetyl-k27-antibody-chip-grade-ab4729.html>

Histone H3 monomethyl (Lys4) (Rabbit Polyclonal, Abcam, ab8895, Lot #GR3312607-2, 5ug for ChIP)
<https://www.abcam.com/products/primary-antibodies/histone-h3-mono-methyl-k4-antibody-chip-grade-ab8895.html>

Histone H3 trimethyl (Lys4) (Rabbit Polyclonal, Abcam, ab8580, Lot #GR3362386-1, 5ug for ChIP)
<https://www.abcam.com/products/primary-antibodies/histone-h3-tri-methyl-k4-antibody-chip-grade-ab8580.html>

anti-rabbit IgG secondary (Goat Polyclonal, Jackson ImmunoResearch Labs, 111-035-003, Lot #164225, 1:10000 WB dilution)
<https://www.jacksonimmuno.com/catalog/products/111-035-003/1000>

anti-mouse IgG secondary (Goat Polyclonal, Jackson ImmunoResearch Labs, 115-035-003, Lot #167353, 1:10000 WB dilution)
<https://www.jacksonimmuno.com/catalog/products/115-035-003/1000>

DCAF5 (Rabbit Polyclonal, Abcam, ab184974, Lot #1037194-2, 1:1000 WB dilution)
<https://www.abcam.com/products/primary-antibodies/dcaf5-antibody-ab184974.html>

DCAF5 (Rabbit Polyclonal, Made in the Roberts Lab, Ab #3, 1:500 WB dilution, 10ug for IP)
<https://www.thermofisher.com/antibody/product/DDB1-Antibody-Polyclonal/A300-462A-T>

DDB1 (Rabbit Polyclonal, Bethyl, A300-462A, Lot #3, 1:1000 WB dilution)
<https://www.thermofisher.com/antibody/product/DDB1-Antibody-Polyclonal/A300-462A-T>

CUL4A (Rabbit Polyclonal, Bethyl, A300-739A, Lot #2, 1:1000 WB dilution)
<https://www.thermofisher.com/antibody/product/Cul4a-Antibody-Polyclonal/A300-739A>

HA-tag (Rabbit Monoclonal, Cell Signaling Technology, 3724, C29F4, Lot #11, 1:1000 WB dilution; 5ug for IP)
<https://www.cellsignal.com/products/primary-antibodies/ha-tag-c29f4-rabbit-mab/3724>

FKBP12 (Rabbit Polyclonal, Abcam, ab24373, Lot #GR3325907-2, 1:1000 WB)

<https://www.abcam.com/products/primary-antibodies/fkbp12-antibody-ab24373.html>
L3MBTL3/KDM1A (Rabbit Polyclonal, Thermo Fisher Scientific, PA5-96628, Lot #YC3859928D, 1:500 WB dilution)
<https://www.thermofisher.com/antibody/product/L3MBTL3-Antibody-Polyclonal/PA5-96628>
L3MBTL3/KDM1A (Rabbit Polyclonal, Novus Biologicals, NBP1-47316, Lot #A1, 5ug for IP)
https://www.novusbio.com/products/l3mbtl3-antibody_nbp1-47316
LSD1/BHC110 (Rabbit Polyclonal, Bethyl, A300-215A, Lot #2, 1:1000 WB dilution)
<https://www.thermofisher.com/antibody/product/BHC110-LSD1-Antibody-Polyclonal/A300-215A>
P300/KAT3B (Rabbit Polyclonal, Abcam, ab10485, Lot #GR208565-26, 1:1000 WB dilution, 5ug for ChIP)
<https://www.abcam.com/products/primary-antibodies/kat3b-p300-antibody-ab10485.html>
c-Myc/N-Myc (Rabbit Monoclonal, Cell Signaling Technology, 13987, D3N8F, Lot #6, 1:1000 WB dilution)
<https://www.cellsignal.com/products/primary-antibodies/c-myc-n-myc-d3n8f-rabbit-mab/13987>

Validation

Antibodies were validated by the manufacturers or validated in previous studies. Statements on antibody validation are present on the manufacturer's website along with relevant citations (see above). Additional validation was done with control IgG as a negative control. DCAF5 Rabbit Polyclonal Abcam ab184974 was validated in the Dcaf5 germline knockout rabbit. For the DCAF5 in house generated antibody, following a prime, boost, boost regimen, test bleeds (two weeks after the last boost) sera were tested by ELISA, using peptide (not coupled to KLH) coated plates, SDS-PAGE/Western blot, and immunoprecipitation from cell lysate for screening. The most optimal rabbits were then selected based on these results for a final boost and terminal bleed. Cocalico Biologicals Inc., then affinity purified peptide specific antibodies from the sera.

Eukaryotic cell lines

Policy information about [cell lines and Sex and Gender in Research](#)

Cell line source(s)

G401 (ATCC-CRL1441), G402 (ATCC-CRL-1440), HCT116 (ATCC-CCL-247), MCF7 (ATCC HTB-22), and 293T (ATCC-CRL-3216) cell lines were purchased from ATCC. TTC549 cells were obtained via MTA from Tim Triche, University of California Los Angeles. MON cells were obtained via MTA from Franck Bourdeaut, Institut Curie. BT16 cells were obtained via MTA from C. David James, Northwestern University. CH22 cells obtained via MTA from The Chordoma Foundation and Bernard E. Weissman, UNC-Chapel Hill.

Authentication

Commercial cell lines from ATCC were authenticated by manufacturer and we authenticated by STR profiling CH22 from Chordoma Foundation. TTC549, BT16 and MON cell lines were not authenticated.

Mycoplasma contamination

All cells were routinely tested for mycoplasma (Gelantis MycoScope PCR Mycoplasma Detection Kit (Cat#MY01100)) and all cells used in this study were free of mycoplasma contamination.

Commonly misidentified lines (See [ICLAC](#) register)

No commonly misidentified cell lines were used in this study.

Animals and other research organisms

Policy information about [studies involving animals; ARRIVE guidelines](#) recommended for reporting animal research, and [Sex and Gender in Research](#)

Laboratory animals

For dTAG-DCAF5 in vivo studies, athymic nude immunodeficient mice were purchased from Charles River (strain code 553; Stress Level: C). Mice were approximately 6-12 weeks in age. For generating the Dcaf5 germline knockout model, six-week-old male and female C57BL/6 mice were purchased from Jackson Laboratory (Stock# 000664). Six-week-old male and female C57BL/6 mice were purchased from Jackson Laboratory (Stock# 000664). Animals were housed on a 12-12 light cycle (light on 6 am off 6pm) and provided food and water ad libitum. Animals are housed in a facility that is 68-70 degrees F (20-22 degrees C) with humidity levels maintained at 30-70% at cage level.

Wild animals

No wild animals were used in this study.

Reporting on sex

It is difficult and challenging to xenograft male mice because randomizing them into other cages with unfamiliar male mice often results in fighting and unnecessary wounds inflicted. For our pilot study females were used as it was more cost effective and they can be randomized more easily into cages.

Field-collected samples

No field collected samples were used in this study.

Ethics oversight

Animal maintenance and procedures were performed in accordance with the National Institutes of Health Guide for the Care and Use of Laboratory Animals. The animal protocol was approved by the Institutional Animal Care and Use Committee at St. Jude Children's Research Hospital under certificate number 595. All efforts were made to minimize suffering. Animal care was facilitated by the Animal Husbandry Unit at St. Jude Children's Research Hospital in accordance with their guidelines and regulations.

Note that full information on the approval of the study protocol must also be provided in the manuscript.

Plants

Seed stocks

No seed stocks were used in this study

Novel plant genotypes

No novel plant genotypes were used in this study.

Authentication

No authentication was conducted since plants were not used in this study

ChIP-seq

Data deposition

- Confirm that both raw and final processed data have been deposited in a public database such as [GEO](#).
- Confirm that you have deposited or provided access to graph files (e.g. BED files) for the called peaks.

Data access links

May remain private before publication.

<https://www.ncbi.nlm.nih.gov/geo/query/acc.cgi?acc=GSE215025>

Files in database submission

Samples (94)

Less... Less...

GSM6620072 G401_ATAC_shCTRL_rep1
 GSM6620073 G401_ATAC_shCTRL_rep2
 GSM6620074 G401_ATAC_shCTRL_rep3
 GSM6620075 G401_ATAC_shDCAF5_rep1
 GSM6620076 G401_ATAC_shDCAF5_rep2
 GSM6620077 G401_ATAC_shDCAF5_rep3
 GSM6620078 G401_shCTRL_Input_rep2 [2418828]
 GSM6620079 G401_shDCAF5_Input_rep2 [2418829]
 GSM6620080 G401_shCTRL_BRG1_rep3 [2418831]
 GSM6620081 G401_shCTRL_ARID1A_rep2 [2418832]
 GSM6620082 G401_shCTRL_ARID1A_rep3 [2418833]
 GSM6620083 G401_shCTRL_BAF155_rep2 [2418834]
 GSM6620084 G401_shCTRL_BAF155_rep3 [2418835]
 GSM6620085 G401_shDCAF5_BRG1_rep2 [2418836]
 GSM6620086 G401_shDCAF5_BRG1_rep3 [2418837]
 GSM6620087 G401_shDCAF5_ARID1A_rep2 [2418838]
 GSM6620088 G401_shDCAF5_ARID1A_rep3 [2418839]
 GSM6620089 G401_shDCAF5_BAF155_rep2 [2418840]
 GSM6620090 G401_shDCAF5_BAF155_rep3 [2418841]
 GSM6620091 G401_shCTRL_H3K27ac_rep2 [2418843]
 GSM6620092 G401_shCTRL_H3K4me3_rep1 [2418844]
 GSM6620093 G401_shCTRL_H3K4me3_rep2 [2418845]
 GSM6620094 G401_shCTRL_H3K4me1_rep1 [2418846]
 GSM6620095 G401_shCTRL_H3K4me1_rep2 [2418847]
 GSM6620096 G401_shDCAF5_H3K27ac_rep1 [2418848]
 GSM6620097 G401_shDCAF5_H3K27ac_rep2 [2418849]
 GSM6620098 G401_shDCAF5_H3K4me3_rep1 [2418850]
 GSM6620099 G401_shDCAF5_H3K4me3_rep2 [2418851]
 GSM6620100 G401_shDCAF5_H3K4me1_rep1 [2418852]
 GSM6620101 G401_shDCAF5_H3K4me1_rep2 [2418853]
 GSM6620102 G401_shCTRL_input_rep1 [2403653]
 GSM6620103 G401_shDCAF5_input_rep1 [2403654]
 GSM6620104 G401_shCTRL_ARID1A_rep1 [2403655]
 GSM6620105 G401_shCTRL_BAF155_rep1 [2403656]
 GSM6620106 G401_shCTRL_BRG1_rep1 [2403657]
 GSM6620107 G401_shDCAF5_ARID1A_rep1 [2403658]
 GSM6620108 G401_shDCAF5_BAF155_rep1 [2403659]
 GSM6620109 G401_shDCAF5_BRG1_rep1 [2403660]
 GSM6620110 G401_shCTRL_BRD9_rep1 [2432992]
 GSM6620111 G401_shCTRL_BRD9_rep2 [2432994]
 GSM6620112 G401_shDCAF5_BRD9_rep1 [2432998]
 GSM6620113 G401_shDCAF5_BRD9_rep2 [2433000]
 GSM6620114 G401_shCTRL_Input_rep1 [2432990]
 GSM6620115 G401_shDCAF5_Input_rep1 [2432991]
 GSM6620116 G401_GFP_shctrl_rep1

GSM6620117 G401_GFP_shctrl_rep2
 GSM6620118 G401_GFP_shctrl_rep3
 GSM6620119 G401_GFP_shdcaf5_rep1
 GSM6620120 G401_GFP_shdcaf5_rep2
 GSM6620121 G401_GFP_shdcaf5_rep3
 GSM6620122 G401_SB1_shctrl_rep1
 GSM6620123 G401_SB1_shctrl_rep2
 GSM6620124 G401_SB1_shctrl_rep3
 GSM6620125 G401_SB1_shdcaf5_rep1
 GSM6620126 G401_SB1_shdcaf5_rep2
 GSM6620127 G401_SB1_shdcaf5_rep3
 GSM7747696 G401 shCTRL input [2516867]
 GSM7747697 G401 shDCAF5 input [2516868]
 GSM7747698 G401 shCTRL p300 AbCam rep1 [2516869]
 GSM7747699 G401 shCTRL p300 AbCam rep2 [2516870]
 GSM7747700 G401 shCTRL p300 AbCam rep3 [2516871]
 GSM7747701 G401 shDCAF5 p300 AbCam rep1 [2516872]
 GSM7747702 G401 shDCAF5 p300 AbCam rep2 [2516873]
 GSM7747703 G401 shDCAF5 p300 AbCam rep3 [2516874]
 GSM7747704 G401 dTAG DCAF5 DMSO input [2574938]
 GSM7747705 G401 dTAG DCAF5 V1 input [2574939]
 GSM7747706 G401 dTAG DCAF5 DMSO 4h ARID1A sigma rep1 [2574941]
 GSM7747707 G401 dTAG DCAF5 DMSO 4h BAF155 thermo rep1 [2574942]
 GSM7747708 G401 dTAG DCAF5 DMSO 4h BRG1 abcam rep1 [2574943]
 GSM7747709 G401 dTAG DCAF5 V1 4h ARID1A sigma rep1 [2574944]
 GSM7747710 G401 dTAG DCAF5 V1 4h BAF155 thermo rep1 [2574945]
 GSM7747711 G401 dTAG DCAF5 V1 4h BRG1 abcam rep1 [2574946]
 GSM7747712 G401dTAGDCAF5 DMSO 4h H3K27ac AbCam rep1 [2585563]
 GSM7747713 G401dTAGDCAF5 DMSO 4h H3K27ac AbCam rep2 [2585564]
 GSM7747714 G401dTAGDCAF5 V1 4h H3K27ac AbCam rep1 [2585565]
 GSM7747715 G401dTAGDCAF5 V1 4h H3K27ac AbCam rep2 [2585566]
 GSM7747786 G401_ATAC_shCTRL_DMSO_rep1
 GSM7747787 G401_ATAC_shCTRL_DMSO_rep2
 GSM7747788 G401_ATAC_shCTRL_DMSO_rep3
 GSM7747789 G401_ATAC_shCTRL_BRM014_rep1
 GSM7747790 G401_ATAC_shCTRL_BRM014_rep2
 GSM7747791 G401_ATAC_shCTRL_BRM014_rep3
 GSM7747792 G401_ATAC_shDCAF5_DMSO_rep1
 GSM7747793 G401_ATAC_shDCAF5_DMSO_rep2
 GSM7747794 G401_ATAC_shDMSO_DMSO_rep3
 GSM7747795 G401_ATAC_shDCAF5_BRM014_rep1
 GSM7747796 G401_ATAC_shDCAF5_BRM014_rep2
 GSM7747797 G401_ATAC_shDCAF5_BRM014_rep3
 GSM7747798 ATAC_G401_dTAGDCAF5_DMSO_4h_rep1
 GSM7747799 ATAC_G401_dTAGDCAF5_DMSO_4h_rep2
 GSM7747800 ATAC_G401_dTAGDCAF5_DMSO_4h_rep3
 GSM7747801 ATAC_G401_dTAGDCAF5_V1_4h_rep1
 GSM7747802 ATAC_G401_dTAGDCAF5_V1_4h_rep2
 GSM7747803 ATAC_G401_dTAGDCAF5_V1_4h_rep3

Genome browser session
(e.g. [UCSC](#))

No longer applicable.

Methodology

Replicates

All ChIP-Seq in shCTRL and shDCAF5 cells were performed with n = 2-3 biological replicates. H3K27ac shCTRL and BRG1 shCTRL had n = 2 due to technical outliers. G401 dTAG-DCAF5 DMSO and V-1 treated ChIP-Seq was performed n=1

Sequencing depth

Sample	Total(M)	Final Read	Fragment Size (bp)	R	S	C	TAG
2418828_G401_shCTRL_Input_S1.hg19	108.1	87.7	130	1.62	2		
2418829_G401_shDCAF5_Input_S2.hg19	76	58.3	130	1.9	2		
2418830_G401_shCTRL_BRG1_abcam_rep2.hg19	107.1	1.5	190	3.07	2		
2418831_G401_shCTRL_BRG1_abcam_rep3_S4.hg19	101.2	74.1	195	1.31	1		
2418832_G401_shCTRL_ARID1A_sigma_rep2_S5.hg19	79.1	53.8	190	1.5	2		
2418833_G401_shCTRL_ARID1A_sigma_rep3_S6.hg19	118	80.1	195	1.53	2		
2418834_G401_shCTRL_BAF155_Thermo_rep2_S7.hg19	82.7	12.3	125	1.51	2		
2418835_G401_shCTRL_BAF155_Thermo_rep3_S8.hg19	110.9	74.2	165	1.27	1		
2418836_G401_shDCAF5_BRG1_abcam_rep2_S9.hg19	99.4	69.7	220	1.45	1		
2418837_G401_shDCAF5_BRG1_abcam_rep3_S10.hg19	131.7	79.7	220	1.56	2		
2418838_G401_shCTRL_ARID1A_Sigma_rep2_S11.hg19	68.7	18.5	200	1.74	2		
2418839_G401_shCTRL_ARID1A_Sigma_rep3_S12.hg19	113.9	77.7	190	1.58	2		
2418840_G401_shDCAF5_BAF155_Thermo_rep2_S13.hg19	85.5	47.2	170	1.64	2		
2418841_G401_shDCAF5_BAF155_Thermo_rep3_S14.hg19	108.4	66.5	170	1.58	2		
2418842_G401_shCTRL_H3K27ac_abcam_rep1.hg19	156.5	4.4	190	2.35	2		
2418843_G401_shCTRL_H3K27ac_abcam_rep2_S16.hg19	146.6	114.7	205	1.38	1		
2418844_G401_shCTRL_H3K4me3_abcam_rep1_S17.hg19	147.1	96.7	285	1.29	1		

2418845_G401_shCTRL_H3K4me3_abcam_rep2_S18.hg19 149.4 106.9 240 1.24 1
 2418846_G401_shCTRL_H3K4me1_abcam_rep1_S19.hg19 65.7 42.4 230 1.88 2
 2418847_G401_shCTRL_H3K4me1_abcam_rep2_S20.hg19 122.2 78.3 225 1.69 2
 2418848_g401_shDCAF5_H3K27ac_abcam_rep1_S1.hg19 137 116.2 215 1.35 1
 2418849_g401_shDCAF5_H3K27ac_abcam_rep2_S2.hg19 133.2 106.6 260 1.39 1
 2418850_g401_shDCAF5_H3K4me3_abcam_rep1_S3.hg19 102.8 71.6 205 1.24 1
 2418851_g401_shDCAF5_H3K4me3_abcam_rep2_S4.hg19 194.2 155.2 195 1.24 1
 2418852_G401_shDCAF5_H3K4me1_abcam_rep1_S5.hg19 148.4 120.5 175 1.49 1
 2418853_G401_shDCAF5_H3K4me1_abcam_rep2_S6.hg19 152.6 123.8 185 1.48 1
 2516867_G401_shCTRL_input_hg19 55.5 41.9 165 0.65 0
 2516868_G401_shDCAF5_input_hg19 70.5 51.7 165 0.77 0
 2516869_G401_shCTRL_p300_AbCam_n1_hg19 40.2 22.9 175 1.26 1
 2516870_G401_shCTRL_p300_AbCam_n2_hg19 64.0 37.4 180 1.39 1
 2516871_G401_shCTRL_p300_AbCam_n3_hg19 58.6 35.1 170 1.37 1
 2516872_G401_shDCAF5_p300_AbCam_n1_hg19 60.7 35.8 175 1.50 1
 2516873_G401_shDCAF5_p300_AbCam_n2_hg19 70.7 31.7 160 1.47 1
 2516874_G401_shDCAF5_p300_AbCam_n3_hg19 61.1 36.4 175 1.38 1
 2574938_G401_dTAG_DCAF5_DMSO_input_hg19 59.9 44.6 145 0.29 -1
 2574939_G401_dTAG_DCAF5_V1_input_hg19 64.5 47.5 140 0.29 -1
 2574940_G401_dTAG_DCAF5_untreated_input_hg19 76.6 55.0 125 0.32 -1
 2574941_g401_dTAG_DCAF5_DMSO_4h_ARID1A_sigma_hg19 60.4 41.5 185 1.13 1
 2574942_g401_dTAG_DCAF5_DMSO_4h_BAF155_thermo_hg19 61.5 41.3 185 1.11 1
 2574943_g401_dTAG_DCAF5_DMSO_4h_BRG1_abcam_hg19 59.0 39.5 190 1.01 1
 2574944_g401_dTAG_DCAF5_V1_4h_ARID1A_sigma_hg19 47.0 33.1 185 1.17 1
 2574945_g401_dTAG_DCAF5_V1_4h_BAF155_thermo_hg19 52.4 36.7 210 1.14 1
 2574946_g401_dTAG_DCAF5_V1_4h_BRG1_abcam_hg19 67.2 45.2 180 1.07 1
 2574947_g401_dTAG_DCAF5_untreated_4h_ARID1A_sigma_hg19 60.0 40.9 185 1.12 1
 2574948_g401_dTAG_DCAF5_untreated_4h_BAF155_thermo_hg19 55.5 38.0 195 1.12 1
 2574949_g401_dTAG_DCAF5_untreated_4h_BRG1_abcam_hg19 76.5 49.7 180 0.97 0
 2585563_G401dTAGDCAF5_DMSO_4h_H3K27ac_AbCam_rep1_hg19 40.5 40.5 185 1.159134 1
 2585564_G401dTAGDCAF5_DMSO_4h_H3K27ac_AbCam_rep2_hg19 58.7 58.7 175 1.154558 1
 2585565_G401dTAGDCAF5_V1_4h_H3K27ac_AbCam_rep1_hg19 52.1 52.1 185 1.130766 1
 2585566_G401dTAGDCAF5_V1_4h_H3K27ac_AbCam_rep2_hg19 33.8 33.8 185 1.118442 1

Antibodies

Refer to Antibodies Section

Peak calling parameters

Peaks were called using MACS219 program with –nomodel -q 0.05 flags (high confidence peaks). Separately, narrow peaks were also called with more relaxed criteria, setting the -q flag to 0.5 (low confidence peaks).

Data quality

Samples were evaluated based on: mapping rate to reference was at >80%, duplicate rate < 30%, total non-duplicated reads are over 20M, fragment size estimated by SPP >100bp, Qtag (based on RSC) > 0, and looking at the signal to noise in IGV shows clear enrichments.

Software

Raw reads in fastq format were processed with Trim-Galore tool. ChIP-Seq reads were mapped to human-drosophila reference hybrid genome (merged hg19/GRCh37.p13 and dm6 genomes) with bwa aln, followed by bwa samse. Cross-Correlation analysis was conducted with SPP. Peaks were called using MACS219 program with –nomodel -q 0.05 flags (high confidence peaks). All heat maps and metaplots of normalized, averaged coverage were generated using deeptools. To perform statistical tests between experimental groups for RNA-Seq, ChIP-Seq, and ATAC-Seq, TMM (trimmed mean of M-values) scale factors are estimated using edgeR and a limma-voom, empirical bayes moderation to establish significant differences.

Flow Cytometry

Plots

Confirm that:

- The axis labels state the marker and fluorochrome used (e.g. CD4-FITC).
- The axis scales are clearly visible. Include numbers along axes only for bottom left plot of group (a 'group' is an analysis of identical markers).
- All plots are contour plots with outliers or pseudocolor plots.
- A numerical value for number of cells or percentage (with statistics) is provided.

Methodology**Sample preparation**

G401-dTAG-DCAF5-YFP-dLuc cells were prepared in a conical in PBS for sorting

Instrument

Aria cell sorter (BD Biosciences)

Software

FlowJo 5.4+ version 10

Cell population abundance

78.8% of G401-dTAG-DCAF5-YFP-dLuc cells were YFP+

Gating strategy

G401-dTAG-DCAF5-YFP-dLuc cells sorted for single cells sized at 45.4, subsequently single cells were treated with DAPI for live/dead percentages, singlets were 86.1% live. Of live cells, sorted for YPF fluorophore where 78.8% of single, live cells were YFP+

Tick this box to confirm that a figure exemplifying the gating strategy is provided in the Supplementary Information.